JYVÄSKYLÄ STUDIES IN BIOLOGICAL AND ENVIRONMENTAL SCIENCE
302

Jonne Seppälä

Structural Studies on Filamin Domain Interactions

JYVÄSKYLÄN YLIOPISTO

JYVÄSKYLÄ STUDIES IN BIOLOGICAL AND ENVIRONMENTAL SCIENCE 302

Jonne Seppälä

Structural Studies on Filamin Domain Interactions

Esitetään Jyväskylän yliopiston matemaattis-luonnontieteellisen tiedekunnan suostumuksella
julkisesti tarkastettavaksi yliopiston Ambiotica-rakennuksen salissa YAA303,
toukokuun 22. päivänä 2015 kello 12.

Academic dissertation to be publicly discussed, by permission of
the Faculty of Mathematics and Science of the University of Jyväskylä,
in building Ambiotica, hall YAA303, on May 22, 2015 at 12 o'clock noon.

UNIVERSITY OF JYVÄSKYLÄ

JYVÄSKYLÄ 2015

Structural Studies on Filamin Domain Interactions

JYVÄSKYLÄ STUDIES IN BIOLOGICAL AND ENVIRONMENTAL SCIENCE 302

Jonne Seppälä

Structural Studies on Filamin Domain Interactions

UNIVERSITY OF JYVÄSKYLÄ

JYVÄSKYLÄ 2015

Editors
Varpu Marjomäki
Department of Biological and Environmental Science, University of Jyväskylä
Pekka Olsbo, Ville Korkiakangas
Publishing Unit, University Library of Jyväskylä

Jyväskylä Studies in Biological and Environmental Science

URN:ISBN:978-951-39-6199-2
ISBN 978-951-39-6199-2 (PDF)

ISBN 978-951-39-6198-5 (nid.)
ISSN 1456-9701

Jyväskylä University Printing House, Jyväskylä 2015

ABSTRACT

Seppälä, Jonne
Structural Studies on Filamin Domain Interactions
Jyväskylä: University of Jyväskylä, 2015, 49 p.
(Jyväskylä Studies in Biological and Environmental Science
ISSN 1456-9701; 302)
ISBN 978-951-39-6198-5 (nid.)
ISBN 978-951-39-6199-2 (PDF)
Yhteenveto: Rakennetutkimuksia filamiini-proteiinin domeenivuorovaikutuksilla
Diss.

Filamins are cytoskeletal proteins that cross-link actin filaments into three-dimensional gel-like meshwork, thereby contributing to the regulation of cell locomotion and membrane integrity. Filamins are also crucial linkers between the cytoskeleton and extracellular matrix by responding to mechanical clues and transforming them into biochemical signals, in a process known as mechanosensory signalling. This is achieved by conformational rearrangements on part of filamin domains. Filamins contain an actin binding domain followed by 24 immunoglobulin-like domains. Mutations along the protein cause developmental disorders affecting the brain, heart, skeleton and muscles. Because filamins have extended shapes and they are flexible, the detailed structure of the full molecule is unknown. However, studies with smaller pieces have revealed that filamins contain three interacting domain pairs, two of which have shown to be mechanically regulated ligand-binding units. The function of the third domain pair is still unknown. In this thesis, by using x-ray crystallography and small-angle x-ray scattering, first, a novel three domain ligand-binding structure of filamins was solved. Second, ligand induced conformational changes on one of the aforementioned mechanically regulated domain pairs were studied, and it was discovered that the ligand-bound domain pair is flexible, but restricted in conformations. This may be an important feature regarding the mechanosensing mediated at the site. Third, structural effects of disease-causing mutations on the domain pair of no known function were inspected, and it was discovered that the mutations destabilise the domain pair, possibly altering its ligand binding ability or potential mechanosensory functions.

Keywords: Filamin, immunoglobulin-like domain, inter-domain interactions, mechanosensing, small-angle x-ray scattering, x-ray crystallography.

Jonne Seppälä, University of Jyväskylä, Department of Biological and Environmental Science, P.O. Box 35, FI-40014 University of Jyväskylä, Finland

Author's address Jonne Seppälä
Department of Biological and Environmental Science
P.O. Box 35
FI-40014 University of Jyväskylä
Finland
jonne.s.seppala@jyu.fi

Supervisors Professor Jari Ylänne
Department of Biological and Environmental Science
P.O. Box 35
FI-40014 University of Jyväskylä
Finland

Docent Ulla Pentikäinen, Ph.D.
Department of Biological and Environmental Science
P.O. Box 35
FI-40014 University of Jyväskylä
Finland

Reviewers Docent Tommi Kajander, Ph.D.
Institute of Biotechnology
Biocenter 3, Viikinkaari 1
P.O. Box 65
University of Helsinki
FI-00014 Helsinki
Finland

Andrew Sutherland-Smith, Ph.D.
Institute of Fundamental Sciences
Massey University
Private Bag 11222
Palmerston North 4442
New Zealand

Opponent Professor Kristina Djinović-Carugo
Max F. Perutz Laboratories
University Departments at the Vienna Biocenter
Department for Biomolecular Structural Chemistry
University of Vienna
Campus Vienna Biocenter 5
A-1030 Vienna
Austria

CONTENTS

LIST OF ORIGINAL PUBLICATIONS

The thesis is based on the following original papers, which will be referred to in the text by roman numerals.

I Sethi, R., Seppälä, J., Tossavainen, H., Ylilauri, M., Ruskamo, S., Pentikäinen, O.T., Pentikäinen, U., Permi, P., and Ylänne, J. 2014. A Novel Structural Unit in the N-terminal Region of Filamins. *Journal of Biological Chemistry*, 289:8588-8598.

II Seppälä, J., Tossavainen, H., Rodic, N., Permi, P., Pentikäinen, U.*, and Ylänne, J.* Flexible structure of Peptide Bound Filamin A Mechanosensor Domain Pair 20–21. (Submitted manuscript)

III Seppälä, J., Haataja, T., Ylänne, J., and Pentikäinen, U. Structural Characterization of Human Filamin Domains 16–17 Patient Mutations Causing Skeletal Dysplasia. (Manuscript)

* equal contribution

CONTRIBUTION OF JONNE SEPPÄLÄ IN THE THESIS ARTICLES

I I cloned, expressed, purified and crystallised FLNa3–5. I collected and analysed respective SAXS data and solved the crystal structure. I performed the sequence conservation analysis, and I participated in writing the article and preparing the figures. This article has also been used as a part of Ritika Sethi's dissertation.

II I purified and crystallised the protein-peptide complex. I collected the diffraction data and solved the structure with Jari Ylänne. I collected the SAXS data with Ulla Pentikäinen and performed the data analysis. I prepared all the figures and wrote the manuscript with contributions from the co-authors.

III I conducted the DNA cloning and mutagenesis. I expressed and purified the proteins together with Tatu Haataja. I crystallised the protein and solved the crystal structure. I conducted the SAXS data collection and analysis with Ulla Pentikäinen. I performed the stability assays and circular dichroism measurements with Tatu Haataja. I prepared the figures and wrote the manuscript with Jari Ylänne and Ulla Pentikäinen.

ABBREVIATIONS

ABD	actin-binding domain
CH	calponin homology
D_{max}	maximum dimension
EOM	ensemble optimization method
FLN	filamin
HSQC	heteronuclear single quantum coherence
NMR	nuclear magnetic resonance
$P(r)$	pair-distance distribution function
R_g	radius of gyration
SAXS	small-angle x-ray scattering

1 INTRODUCTION

In order to function properly, cells must be able to control their shape, organise internal structures, move, and interact with their environment. These depend heavily on the cytoskeleton, which is composed of three families of filamentous proteins: intermediate filaments, microtubules and actin filaments, all with well-defined roles. Actin filaments are responsible for cell shape and locomotion. Diverse actin binding proteins function in conjunction with actin to regulate actin filament dynamics. One family of such proteins are filamins (FLNs). FLNs are actin cross-linking proteins that help in stabilising the actin network into three-dimensional gel-like sheets essential for lamellipodia formation. In addition, FLNs function as scaffolds during signalling and are partially responsible for the mechanosensitivity of cells.

This thesis centres on the structures of FLNs and what the structure tells about the function. The latter is approached by examining how the internal organisation of FLNs regulates the ligand binding and what consequences disease-associated mutations have on the structures.

1.1 Biological relevance of filamins

FLNs were originally discovered in rabbit (Hartwig and Stossel 1975) and chicken tissues (Wang *et al.* 1975), and they were found to be potent actin gelators with a filamentous multi-domain structure (Gorlin *et al.* 1990). The FLN protein family spans the animal kingdom. Besides vertebrates, FLN orthologues have been described for *Drosophila melanogaster,* fruit fly (Sokol and Cooley 1999); *Caenorhabditis elegans,* roundworm (Wilson *et al.* 1994); *Dictyostelium discoideum,* amoebic slime mould (Hock and Condeelis 1987); and *Entamoeba histolytica,* parasitic protozoan (Vargas *et al.* 1996). The domain composition and overall architecture of the protein varies depending on the species. Generally, the primitive species have fewer domains than vertebrates (Van Der Flier and Sonnenberg 2001) and a comparison of FLN sequences shows that the domains in higher eukaryotes have evolved via multiple tandem duplications (Light *et*

al. 2012). These findings suggest that FLNs evolved early, along with actin-based amoeboid motility mechanisms (Fritz-Laylin *et al.* 2010). No FLNs have been described for plant or fungi.

There are three human FLN encoding genes: x chromosomal FLNA, autosomal FLNB (Takafuta *et al.* 1998) and FLNC (Maestrini *et al.* 1993). All three genes are highly conserved, and their respective proteins (FLNa, FLNb and FLNc) have a near 70% sequence identity. FLNa is the most studied isoform and considered widely to be ubiquitously expressed (Van Der Flier and Sonnenberg 2001). The two other isoforms are more restricted in expression (Takafuta *et al.* 1998; Robertson and Daniel 2012), FLNc being a skeletal and cardiac muscle-specific isoform located within intercalated discs in cardiac muscles and myotendinous junctions in skeletal muscles (Van Der Ven *et al.* 2000). All isoforms, however, are broadly expressed during foetal development and several disease states relating to defects in functions of the proteins arise from mutations in the genes (Robertson and Daniel 2012).

The existence of a wide range of developmental malformations primarily affecting the brain, heart, bone and limbs suggests, and has in part contributed to understanding, that FLNs are involved in the regulation of many cellular processes besides their actin cross-linking ability. Indeed, FLNs function as scaffolds during signal transduction, regulate cell adhesion, migration and extracellular matrix composition, and mediate mechanosensation, which has received increased interest in the field (Zhou *et al.* 2010; Nakamura *et al.* 2011; Razinia *et al.* 2012).

Thus, the study of FLNs not only contributes to understanding how the dynamic actin cytoskeleton is regulated, but also how multi-domain proteins regulate various cellular processes and how their malfunctions give rise to a multitude of developmental disorders.

1.2 General structure of filamins

Vertebrate FLNs are large (240–280 kDa) rod-like proteins with two polypeptide chains (Fig. 1). Each polypeptide chain is composed of an amino terminal actin binding domain (ABD) followed by a string of 24 homologous domains having an immunoglobulin-like fold (Gorlin *et al.* 1990; Fucini *et al.* 1997). These repeat domains are generally divided into two rod segments separated by a flexible hinge region of 25–52 residues that is not predicted to have secondary structure elements. Rod 1 comprises domains 1–15 and rod 2 comprises domains 16–23. There is a second hinge region of 32–40 residues between domains 23 and 24 (Gorlin *et al.* 1990; Van Der Flier and Sonnenberg 2001). Carboxyl terminal domain 24 mediates self-association between the FLN polypeptide chains and forms an FLN dimer that is needed for actin cross-linking (Gorlin *et al.* 1990; Himmel *et al.* 2003; Pudas *et al.* 2005; Seo *et al.* 2009).

The hinge regions bring additional flexibility to the rod segments and in part contribute to the FLN's cross-linking ability of dispersed actin filaments

(Zhou *et al.* 2010). For example, hinge 1 is needed for the elasticity of FLN cross-linked actin filaments against stresses (Gardel *et al.* 2006). Hinge 2, by contrast, is involved in the efficacy of the dimerization of two FLN polypeptide chains (Himmel *et al.* 2003). In addition, a recent study revealed that a short additional hinge region between the ABD and first repeat domain confers additional flexibility that may facilitate actin binding of the ABD (Sawyer and Sutherland-Smith 2012). Rod 1 contributes to actin binding instead. Domains 1–8 are thought to provide additional flexibility that enables actin binding of the following domains upon initial binding of the ABD. Secondary actin binding is needed for high avidity binding of FLNs to actin (Nakamura *et al.* 2007). By contrast, the rod 2 domains do not contribute to actin binding but are available to interact with other proteins. Indeed, a vast majority of the over 90 FLN binding partners characterised thus far are mapped to rod 2 (Nakamura *et al.* 2011).

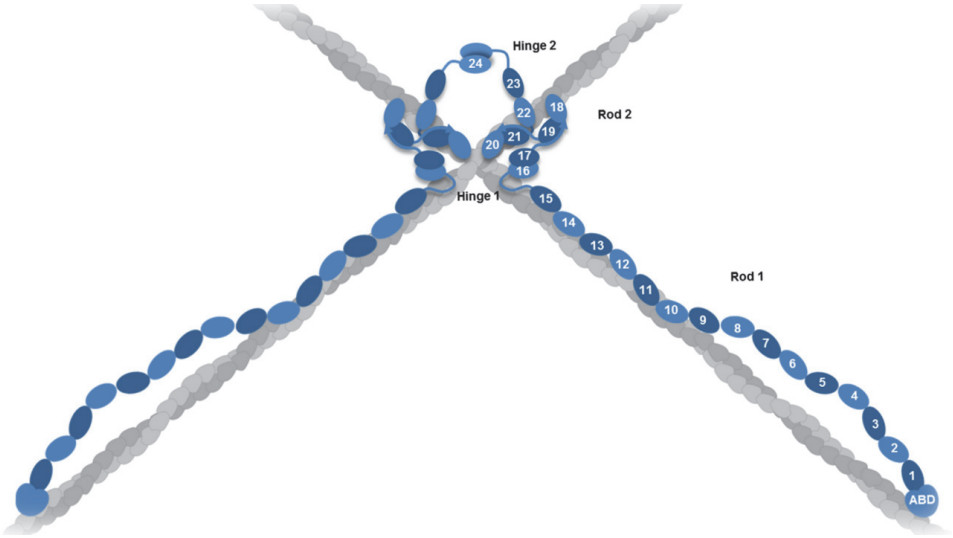

FIGURE 1 A schematic of an FLN dimer (blue) bound to actin filaments (grey). Each polypeptide chain has an amino terminal ABD trailed by 24 FLN immunoglobulin-like domains. These domains are divided into two rods. Hinge regions flank rod 2. The dimerization occurs through the carboxyl terminal end. Known inter-domain interactions in rod 2 are shown.

FLNc differs from the two isoforms by having an additional-81 residue extension in domain 20 that targets muscle sarcomeres (Xie *et al.* 1998; Van Der Ven *et al.* 2000). Alternative splicing brings additional diversity on the structures of the three isoforms. The majority of the splicing affects the rod 2 domains (Zhou *et al.* 2010). For instance, FLNa and b have a splice variant deleting parts of domains 19–20 (Van Der Flier and Sonnenberg 2001). In addition, some splice variants of FLNb and c lack the first hinge region (Van Der Flier *et al.* 2002).

In electron micrography images, functional FLNa dimer adopts a V- or Y–shaped structure (Fig. 1) with a near perpendicular angle between the two polypeptide chains (Gorlin *et al.* 1990; Nakamura *et al.* 2007). The average length of rod 1 measured from the images corresponds nicely with the expected length of 15 Ig-like domains arranged as a string. However, the measured length of rod 2 is shorter than that expected for eight domains, suggesting peculiar domain arrangements (Nakamura *et al.* 2007). Indeed, rod 2 domains 16–21 are shown to form a propeller-like structure, where each of the three blades is composed of two neighbouring domains interacting with each other (Tossavainen *et al.* 2012; Ruskamo *et al.* 2012). The detailed structures of these domain pairs are discussed in the following sections.

1.3 The actin-binding domain

Crystal structures of FLNa and b ABDs have been solved (Clark *et al.* 2009; Ruskamo and Ylänne 2009; Sawyer *et al.* 2009; Sawyer and Sutherland-Smith 2012; PDB code 3FER, Northeast Structural Genomics consortium). The FLN ABD is similar to those found in other actin cross-linking proteins such as α–actinin, fimbrin and plectin (García-Alvarez *et al.* 2003; Klein *et al.* 2004; Franzot *et al.* 2005). It is composed of two calponin-homology domains, CH1 and CH2, connected by a flexible linker (Fig. 2). The CH domain is α helical structure with four major (A, C, E and G) and two short (B and F) helices connected via long flexible loops. The CH domains interact with each other via several salt bridges and are packed closely forming a compact structure. Altogether, there are three actin binding sites, two of which lie in CH1 and one in CH2 (Ruskamo and Ylänne 2009; Sawyer *et al.* 2009). Mutation and truncation studies on several α–actinin-like ABD family members suggest that the full ABD is needed for proper actin binding. Most of the studies imply that the second actin binding site is needed for actin binding, whereas the third one contributes to the binding avidity (Bresnick *et al.* 1991; Hemmings *et al.* 1992; Kuhlman *et al.* 1992; Gimona *et al.* 2002).

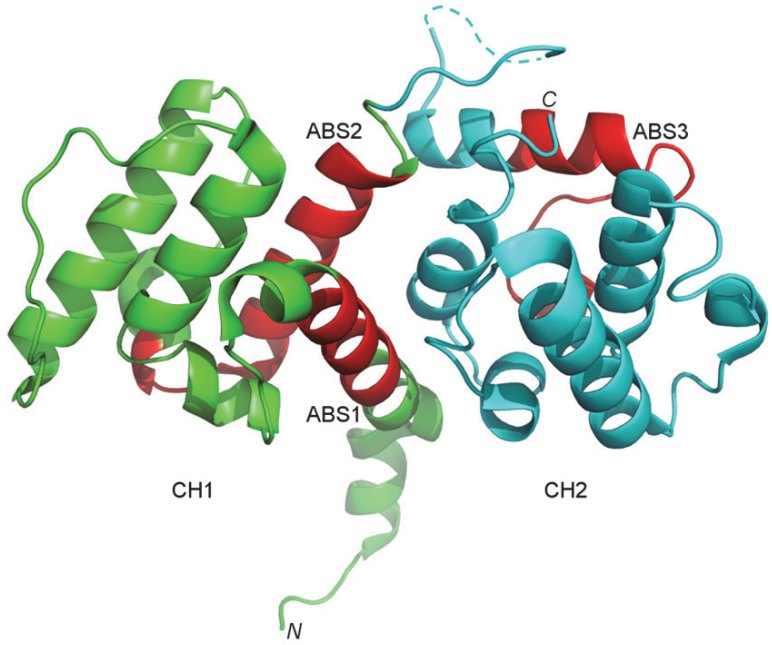

FIGURE 2 Crystal structure of the FLNb ABD (PDB code 2WA5). The two CH domains are coloured green and cyan. The three actin binding sites (ABS) are shown in red.

1.4 Filamin immunoglobulin-like domains

Filamin rod repeats belong to the E set domains in the immunoglobulin superfamily and form a β sandwich fold (Fucini *et al.* 1997; Pudas *et al.* 2005). The domain is composed of two anti-parallel β sheets with strands A, B, D and E forming a four-stranded sheet and strands C, F and G forming a three-stranded sheet (Fig. 3). The domains are approximately 100 residues long (Gorlin *et al.* 1990), except for FLNc20 (Xie *et al.* 1998), as discussed above. Usually, the A strand is interrupted by a 3_{10} helix. However, domains 16, 18 and 20 all lack this helical structure in the segment corresponding the A strand, but are either unstructured (domain 16) (Heikkinen *et al.* 2009) or form peculiar inter-domain interactions with the following domain (domains 18 and 20) (Lad *et al.* 2007; Heikkinen *et al.* 2009). Through detailed sequence analysis, the domains are divided into four subgroups A–D, of which group A domains have a conserved ligand-binding site (Ithychanda *et al.* 2009), which is discussed in detail in section 1.6.

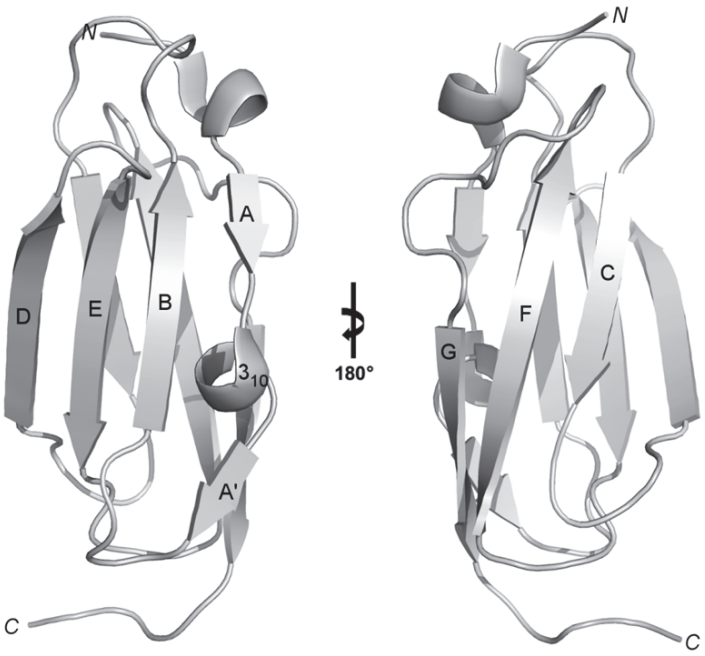

FIGURE 3 A common structure of FLN immunoglobulin-like domain (crystal structure of FLNc23, PDB code 2NQC). The domain is composed of two antiparallel β sheets covering strands ABED and CFG. The A strand is interrupted with a 3_{10} helix.

1.5 Inter-domain interactions in filamins

Multi-domain proteins may be organised as beads-on-a-string, with one domain following another without stable domain-domain interactions or the following domains may interact with each other (Vogel *et al.* 2004). FLNs exhibit features of both of the above, although thus far domain-domain interactions have only been found between two consecutive domains in sequence. In the rod 2 region of FLNs, three domain pairs (domains 16–17, 18–19 and 20–21) form atypical inter-domain interactions (Lad *et al.* 2007; Heikkinen *et al.* 2009). Recently, rod 1 domains 11–12 and 14–15 of FLNc were reported to form putative inter-domain interactions (Sethi and Ylänne 2014).

1.5.1 Domain pair 16–17

The first two domains in rod 2 of FLNa form a tightly interacting domain pair. The segment corresponding to the A strand in most FLN repeats is unstructured in domain 16, which reveals the hydrophobic core at the face formed by B and G strands. This face forms a large interaction surface that is buried by the A and G strands of domain 17 and contains several aromatic and

hydrophobic residues. Hence, the domains lie in parallel next to each other with a relatively large interaction surface area of 720 Å^2 (Fig. 4) (Heikkinen *et al.* 2009).

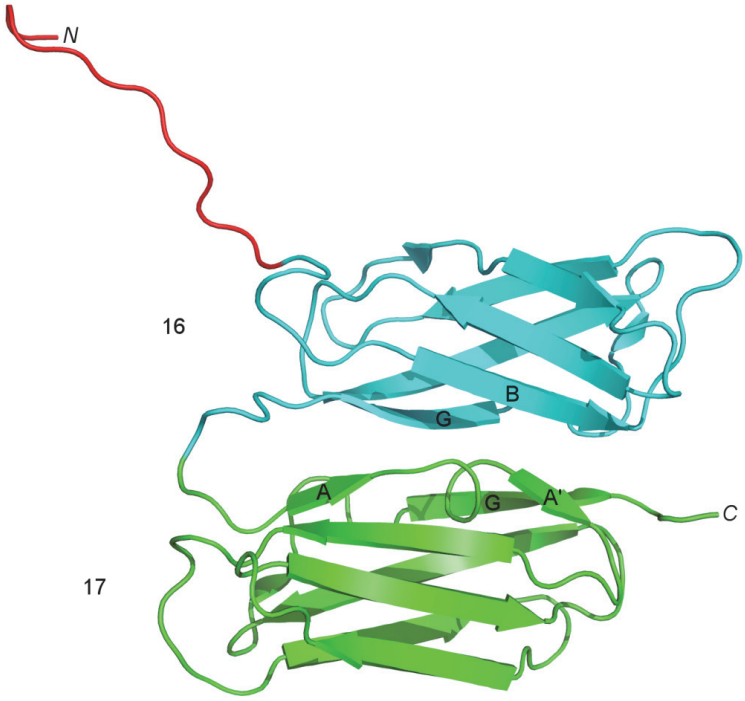

FIGURE 4 Structure of FLNa16–17 (PDB code 2K7P). FLNa16 is shown in cyan and 17 in green. The domains interact via the BG face of domain 16 and AG face of domain 17. Note the unstructured segment corresponding the A strand in domain 16 (in red).

1.5.2 Domain pairs 18–19 and 20–21

In domain pairs 18–19 and 20–21, the A strands of the even numbered domains are folded along the face formed by C and D strands of the odd numbered domains (Fig. 5). The A strand forms an additional β strand to the CFG sheet of the neighbouring domain. This leads to L–shaped structures, where the even numbered domain lies on top of the odd numbered domain roughly perpendicularly to its longitudinal axis. As the A strands of domains 18 and 20 are not folded along the rest of the domain, the hydrophobic core of the domains are exposed, as for domain 16. In domain pair 18–19, the BC loop of domain 19 buries the exposed core of domain 18. As for domain pair 20–21, the BC loop of domain 21 interacts with the G strand of domain 20, leaving the hydrophobic core of domain 20 partially exposed (Lad *et al.* 2007; Heikkinen *et al.* 2009).

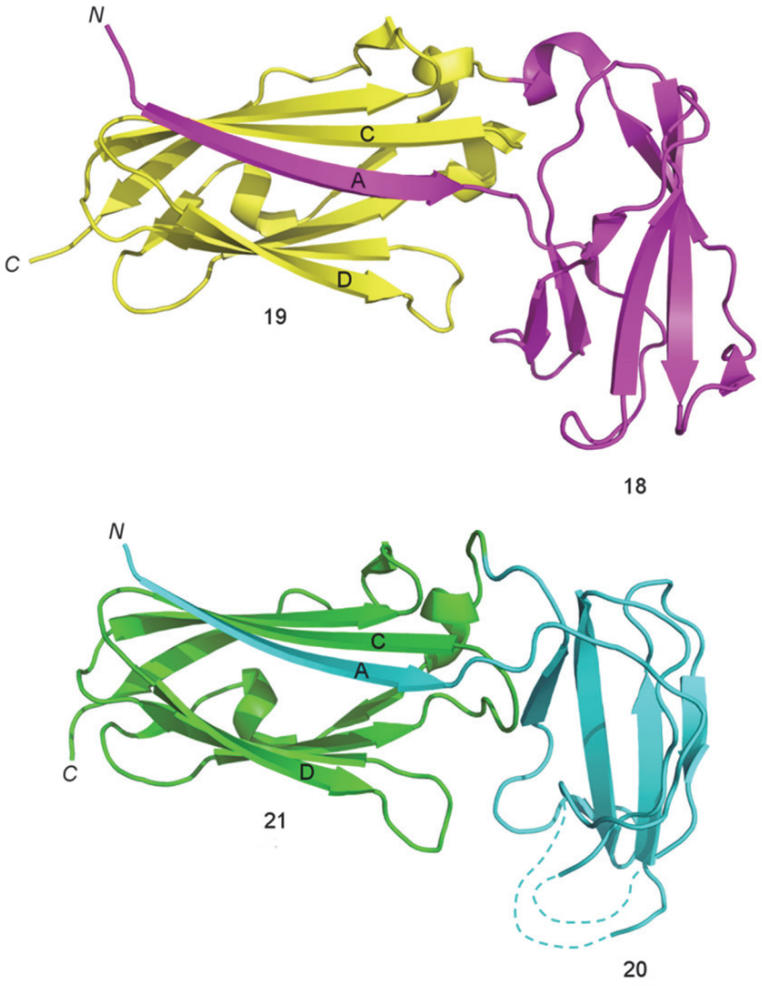

FIGURE 5 Structure of FLNa18–19 (PDB code 2K7Q) and 20–21 (2J3S). The domain pairs are similar in structure. Note that the A strand of the even-numbered domains (18 in magenta and 20 in cyan) folds along the CD face of the odd-numbered domains (19 in yellow and 21 in green). Consequently, the even-numbered domains lie on top of the odd-numbered domains leading to an L-shaped structure.

1.5.3 The dimerization domain

The carboxyl terminal domain mediates the dimerization of FLN polypeptide chains (Gorlin *et al.* 1990) by interacting with its counterpart through the CD face (Fig. 6) (Pudas *et al.* 2005; Seo *et al.* 2009). The interaction has both polar and hydrophobic characteristics. The domains are faced towards each other in an anti-parallel fashion, so that the D strands of the interacting domains are connected to form a single eight-stranded β sheet structure. This leads to a large

interaction interface with 1109 Å^2, almost a fifth of the accessible surface area of the monomeric domain (Pudas *et al.* 2005).

In yeast two-hybrid assays, it was found that, besides domain 24, there might be an additional site in rod 2 that facilitates association between two FLN subunits (Sheen *et al.* 2002). This is supported by single particle electron microscopy experiments, where it was discovered that the segment of domain 16–24 forms a parallel structure, suggesting that other interactions in addition to the dimerization via domain 24 may occur (Ruskamo *et al.* 2012). Indeed, a compensatory dimerization mechanism seems to be mediated via domains 16–23, independent of domain 24 (van Kogelenberg *et al.* 2015).

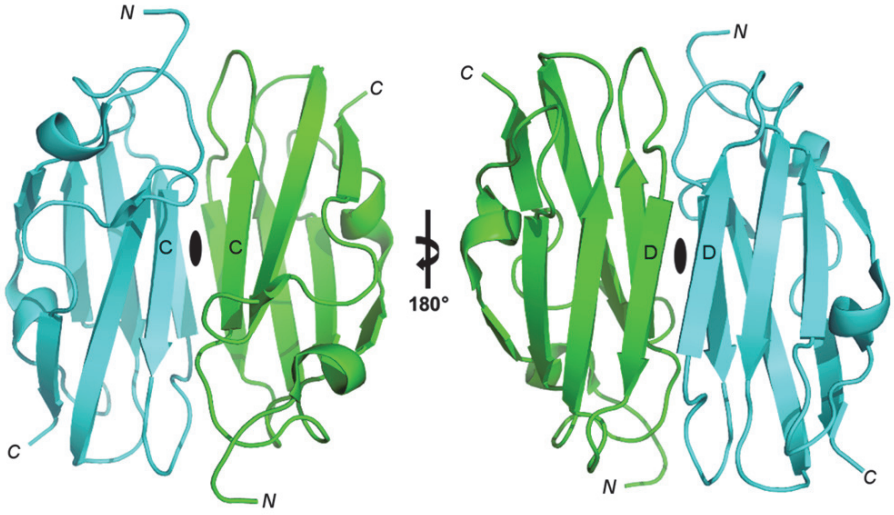

FIGURE 6 Structural basis for FLN dimerization. In the crystal structure of FLNc24 (PDB code 1VO5), the two domains (one in cyan and the other in green) interact with each other through their CD faces (indicated with the black oval). The C and D strands of the domains are connected leading to anti-parallel orientation of the domains.

1.6 Common ligand-binding mechanism

As briefly stated in section 1.1, FLNs interact with numerous proteins of different functions. These include membrane receptors, intracellular signalling proteins, ion channels, enzymes, cytoskeletal and adhesion proteins as well as transcription factors (Nakamura *et al.* 2011). Still, complex structures of FLN domains and their binding partners are limited. Structures are available for individual FLN domains and peptides derived from cytoplasmic tails of membrane receptors β integrins (Kiema *et al.* 2006; Takala *et al.* 2008), glycoprotein Ibα (Nakamura *et al.* 2006), adhesion adaptor protein migfilin (Lad *et al.* 2008) and cystic fibrosis transmembrane conductance regulator chloride

channel (Smith *et al.* 2010). Interestingly, they all have a similar mode of interaction.

The ligand-peptides interact with FLN domains via a mechanism called β sheet augmentation. The bound peptide forms an additional anti-parallel β strand next to C strand, extending the CFG sheet of FLN domain (Fig. 7). The peptide interacts with the hydrophobic groove between the C and D strands, termed as the CD face. The peptide forms several main chain hydrogen bonds with the C strand that may account for the majority of the interaction energy (Razinia *et al.* 2012). However, the specificity of binding is determined by the side chain interactions. Five alternating hydrophobic residues point toward the groove and form either a single hydrogen bond or several hydrophobic interactions with the domain (Kiema *et al.* 2006; Nakamura *et al.* 2006; Takala *et al.* 2008; Lad *et al.* 2008; Smith *et al.* 2010; Razinia *et al.* 2012).

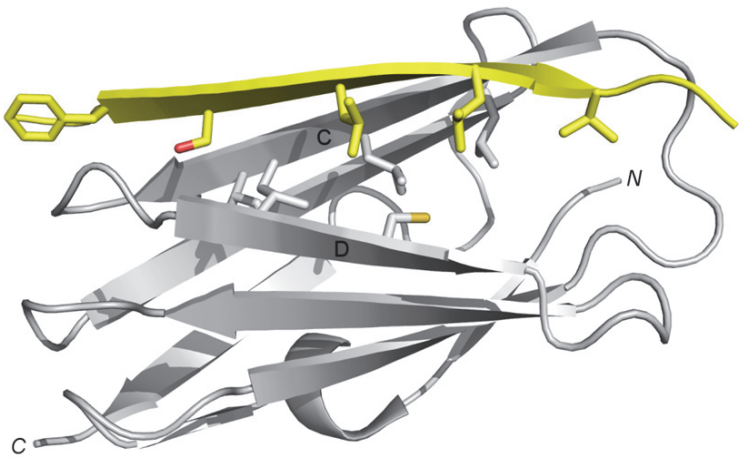

FIGURE 7 Common ligand-binding mechanism on FLNs. Structure of platelet glycoprotein Ibα bound to FLNa17 (PDB code 2BP3) is used here as an example. Ligand-peptides interact with FLN immunoglobulin-like domains through β sheet augmentation. The peptide (in yellow) forms an additional β strand next to the C strand of FLN domain and alternating hydrophobic residues interact with the hydrophobic groove (residues shown as sticks) between the C and D strands.

In addition to the structures mentioned above, a similar binding was verified for signalling intermediate FilGAP, an FLNa-binding GTPase-activating protein, by mutagenesis and NMR chemical shift mapping (Nakamura *et al.* 2009). Furthermore, since the FLN domain binding motif is characteristic β strand forming sequence, it has been used to seek and model binding sequences of known binding partners *in silico* (Li *et al.* 2010; Lamsoul *et al.* 2011).

Altogether, the evidence suggests that the β sheet augmentation to FLN domain CD face represents a common ligand-binding mechanism (Kiema *et al.* 2006; Nakamura *et al.* 2006; Takala *et al.* 2008; Lad *et al.* 2008; Smith *et al.* 2010; Razinia *et al.* 2012). However, many of the reported FLN binding partners do

not have sequences corresponding to the β strand forming motif suggesting that alternative mechanisms for ligand binding on FLN domains exist (Razinia *et al.* 2012).

1.7 Filamins as cellular mechanosensors

Tissue architecture and cell differentiation are regulated by mechanical forces. The cells must be able to sense and respond to different mechanical clues. This phenomenon is termed mechanosensor signalling, which eventually depends on force-induced changes in protein conformation. This, in turn, leads to changes in protein activity, ligand binding and stability. Many mechanically regulated proteins are parts of the cytoskeleton (Vogel and Sheetz 2006).

Mechanosensing has two faces: on the one hand, the cells respond to forces applied from outside. This is powerfully exemplified in hearing, where the waves lead to the mechanical opening of ion channels in the inner ear hair cell stereocilia (Martinac 2004). On the other hand, the cells have a sense of touch by monitoring the differences in forces generated by the cell itself. This accounts for sensing the strength of pulling forces that cells generate to probe the stiffness of the environment in locomotion and adhesion processes (Vogel and Sheetz 2006). Stiffness of the extracellular matrix is a known regulator of cell differentiation (Engler *et al.* 2006). The endogenous pulling forces result from cytoskeletal contractility, namely, acto-myosin contraction. Myosin tenses actin filaments, and the resulting traction forces are ultimately transferred to the extracellular matrix (Vogel and Sheetz 2006). FLNs serve as a link between the actin cytoskeleton and extracellular matrix by anchoring actin filaments to cell surface receptors, such as integrins (Razinia *et al.* 2012). This places FLNs as potential sensors of mechanical forces.

The first evidence for mechanoresponsive properties for FLNs came from experiments showing that FLNa protects the cells from integrin-mediated forces by stabilising the plasma membrane and the cell cortex (Glogauer *et al.* 1998). Soon, it was discovered that FLNa is also central to cell survival by preventing force-induced membrane depolarisation (Kainulainen *et al.* 2002). Direct evidence for mechanosensing function of FLNa came when FLNa–β1 integrin complex was reported to modulate cell contractility in response to matrix stiffness (Gehler *et al.* 2009). Recently, FLNa was also found to stabilise the cell-matrix adhesions under force (Pinto *et al.* 2014). Through application of several force spectroscopy techniques, individual FLN immunoglobulin-like domains were found to undergo partial unfolding in response to pulling forces (Furuike *et al.* 2001; Yamazaki *et al.* 2002; Kolahi and Mofrad 2008). The unfolding is reversible and refolding occurs when the force is reduced to near zero (Furuike *et al.* 2001). The stretching of the domains brings additional flexibility to FLNs and protects the linkage between actin filaments and the cell membrane (Yamazaki *et al.* 2002). Partial unfolding of the domains is also a way to convert force sensing into a biochemical signal via modulation of interactions with

ligands (Lad *et al.* 2007; Razinia *et al.* 2012). The molecular basis for this was discovered in the rod 2 domain pairing, introduced in section 1.5.2.

The function of the first β strand of even-numbered domains 18 and 20 is to hide the common ligand-binding interface – the CD face – of the adjacent odd-numbered domains (Lad *et al.* 2007; Heikkinen *et al.* 2009). Biochemical analyses have demonstrated that the A strand inhibits ligand binding to domains 19 and 21 and that weakening of the A strand interactions by mutations promotes ligand binding (Lad *et al.* 2007). As the inhibitory A strand is folded along the adjacent domain, the termini of the domains are located at the same end of the domain pair. Thus, pulling forces transmitted through the domains may cause the A strand to unfold in a zipper-like fashion, releasing the ligand-binding interface (Fig. 8) (Razinia *et al.* 2012).

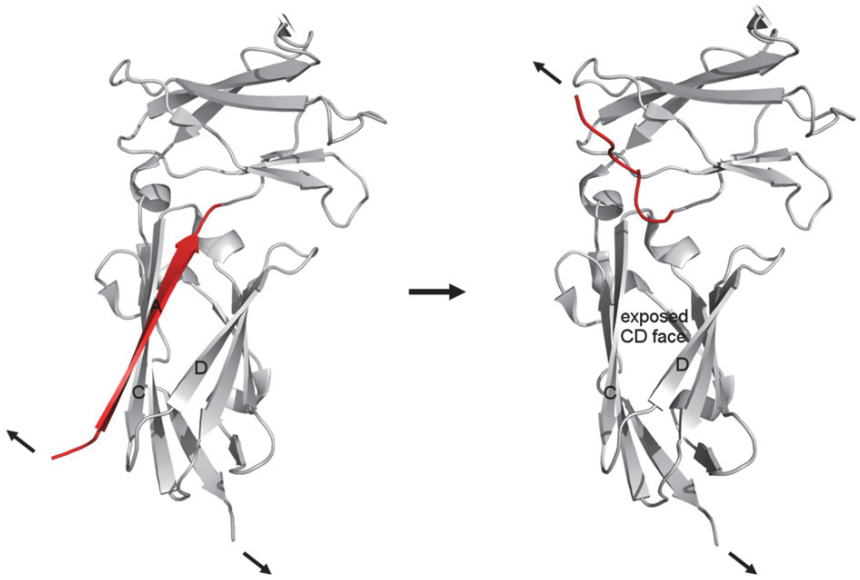

FIGURE 8 Mechanism for the force-induced exposure of the ligand-binding CD face of domains 19 and 21 (shown with structure of FLNa18–19, PDB code 2K7Q). As the termini of the domain pair are at the same end, pulling forces (indicated with the arrows) may cause the CD face masking A strand (in red) to be replaced in a zipper-like fashion, making the CD face open for interactions with ligands.

Steered molecular dynamics simulations on the domain pairs showed gradual exposure of the ligand-binding interfaces upon application of pulling forces (Pentikäinen and Ylänne 2009). Later, single molecule force spectroscopy measurements in domain pair 20–21 demonstrated that A strand detachment occurs at a force range (2–5 pN) capable of being produced by single myosin motors (Rognoni *et al.* 2012). Indeed, myosin-driven actin contraction was shown promote integrin binding on FLNa *in vitro* (Ehrlicher *et al.* 2011), and recently, ligand-binding promoting changes in the 20–21 domain pair

organization were reported to happen in actively protruding leading cell edges (Nakamura *et al.* 2014).

Thus, it is now evident that ligand-binding on at least two FLN domains (19 and 21) can be regulated by pulling forces. On the other hand, it has been demonstrated that FLNs mediate essential mechanoprotective functions in cells.

1.8 Filamin-related diseases

In light of the evidence of how FLNs are mechanosensitive proteins regulating cell motility and signalling, it is not surprising that FLNs are also reported to play a role in cell differentiation and morphogenesis (Zhou *et al.* 2010), processes in which the mechanical cues from the local environment are crucial for them to progress normally. Furthermore, this subjects FLNs as candidate genes for developmental disorders. That said, mutations in all three FLN genes cause a wide spectrum of rare congenital developmental disorders with broad phenotypic consequences that confer to both loss- and gain-of-function effects on the protein (Zhou *et al.* 2010; Robertson and Daniel 2012) (Fig. 9).

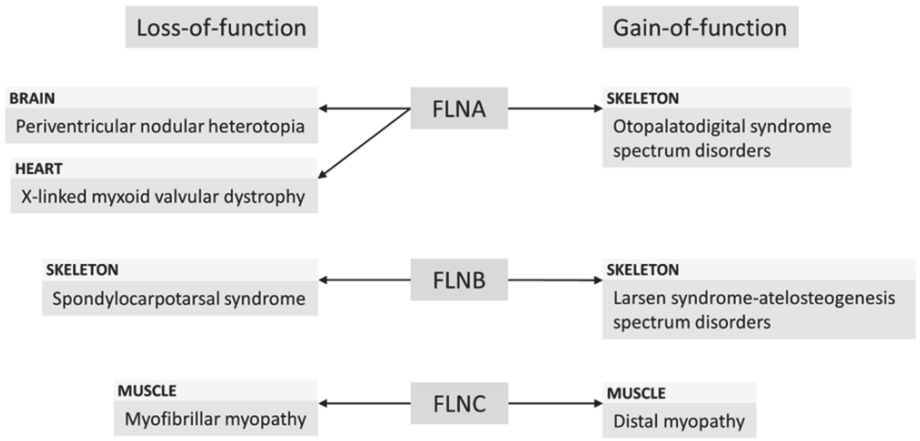

FIGURE 9 Human genetic diseases linked with mutations in FLNs. The mutations cause a diverse array of developmental malformations primarily affecting the brain, heart, skeleton, and muscle.

Nonsense mutations in FLNA lead to a brain malformation known as periventricular nodular heterotopia (Fox *et al.* 1998) and a cardiovascular disease called X-linked myxoid valvular dystrophy (Kyndt *et al.* 2007). Missense mutations in FLNA, by contrast, lead to otopalatodigital spectrum disorders, which are primarily associated with defects in the skeleton (Robertson 2007). Nonsense mutations in FLNB cause spondylocarpotarsal syndrome (Langer *et al.* 1994) and missense mutations in Larsen syndrome–atelosteogenesis spectrum disorders, both causing severe skeletal malformations (Krakow *et al.*

2004; Bicknell *et al.* 2005). Finally, mutations in FLNC develop skeletal and cardiac muscle dysfunctions known as myofibrillar myopathy and distal myopathy, characterised by slow progressive muscle weakness (Vorgerd *et al.* 2005; Duff *et al.* 2011).

Current understanding of the molecular level mechanisms behind these disorders is still relatively poorly understood (Robertson and Daniel 2012). However, many of the phenotypic consequences of the mutations match possible defects in mechanosensory functions of FLNs (Sutherland-Smith 2011). Further studies are required to explain the structural consequences of the mutations on FLNs and how they alter the function and downstream pathways. Interestingly, although mutations span the protein, many disease-specific mutations seem to cluster in particular locations in FLNs (Fig. 10) giving a clue to the possible pathophysiological mechanisms (Parrini *et al.* 2006; Robertson *et al.* 2006; Kyndt *et al.* 2007; Robertson 2007; Fürst *et al.* 2013; Duval *et al.* 2014). The majority of the mutations in FLNC are found in the ABD or the dimerization domain (repeat 24) and cause either truncated or misfolded protein that forms large cytoplasmic aggregates in muscle fibres (Vorgerd *et al.* 2005; Duff *et al.* 2011; Kley *et al.* 2012). Similarly, FLNA and FLNB gain- and loss-of-function mutations are found in the ABD and are predicted to alter actin binding affinity (Robertson *et al.* 2003; Clark *et al.* 2009; Sawyer *et al.* 2009; Daniel *et al.* 2012). Many of the mutations also cluster to the immunoglobulin-like domains, whose function and binding partners are not well characterised. Notably, among these domains are the ones known or predicted to form inter-domain interactions and participate in high avidity actin binding. Possible mechanisms behind the disorders could be an altered force response due to conformational rearrangements that in turn affect downstream signalling pathways. Weakened actin binding might lead to premature FLN dissociation from actin, which would break the mechanical linkage between the cytoskeleton and extracellular matrix. Enhanced actin cross-linking activity in contrast could lead to increased force-induced stiffening of the actin network (Sutherland-Smith 2011).

Taken together, FLNs have a central role in regulating mechanical signals during development, and deficiencies with these signals are associated with several congenital disorders. A study of the underlying mechanisms can help understand the role of FLNs as molecular springs.

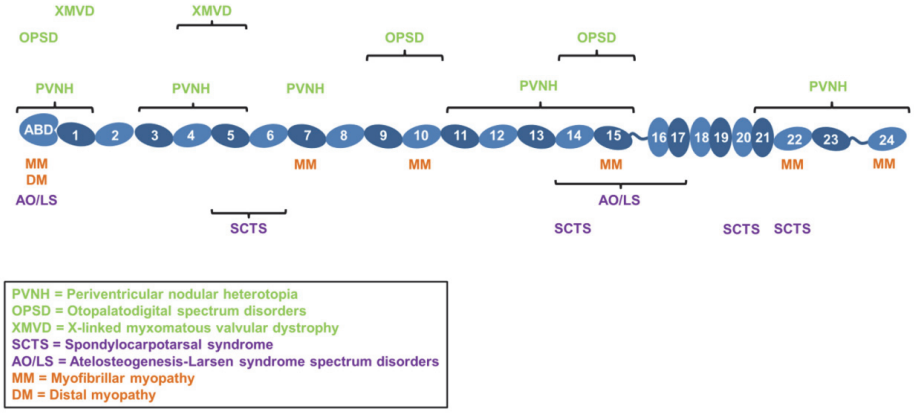

FIGURE 10 Clustering of disease-causing mutations on human FLN isoforms. Although mutations are found over the length of the protein, disease-specific clustering of mutations is observed (FLNa-related diseases are marked with green, FLNb with magenta, and FLNc with orange).

2 AIMS OF THE STUDY

Over recent years, the knowledge on detailed structural arrangements on the FLN rod domains has increased significantly with the discovery of domain pairing, and this has contributed to the understanding of mechanosensory functions of FLNs. The full picture of how the domain pairs contribute to mechanosensing and whether more of such domain arrangements exist is unknown. With this in mind, the aims of the research conducted in this thesis were as follows:

I To study whether domain-domain interactions exist in the N terminal region of FLNs and whether they regulate ligand binding.

II To test how ligand binding changes the conformation of the mechanosensory domain pair 20–21 of FLNa.

III To test how human patient mutations alter the structure of the FLN domain pair 16–17.

3 SUMMARY OF THE METHODS

TABLE 1 Summary of the methods used in the thesis. Detailed descriptions can be found in the original publications.

Method	Publication
Conventional cloning	II
Ligation independent cloning	I, III
Site-directed mutagenesis	III
Bacterial protein expression	I, II, III
Protein purification	I, II, III
SAXS data collection and processing	I, II, III
SAXS *ab initio* and rigid body modelling	I, II, III
EOM	I, II
Crystallisation	I, II, III
X-ray diffraction data collection and processing	I, II, III
Structure determination and refinement	I, II, III
NMR measurements*	I, II
Thermal stability assay	I, III
Sequence alignment	I, II

*The NMR measurements were performed by M.Sc. Nebojsa Rodic and Drs Helena Tossavainen and Perttu Permi.

4 RESULTS AND DISCUSSION

4.1 Filamin domains 3–5 form novel and conserved inter-domain interactions (I)

As discussed in section 1.5, the FLN immunoglobulin-like domains are not all arranged simply as beads-on-a-string. The C-terminal rod 2 region domains 16–17, 18–19, and 20–21 in FLNa form interacting domain pairs (Lad *et al.* 2007; Heikkinen *et al.* 2009). The function of even-numbered domains 18 and 20 is to hide the ligand-binding site on the following domain providing auto-inhibitory mechanism of ligand binding. These interactions can be revealed by external pulling forces or the ligand itself (Lad *et al.* 2007; Pentikäinen and Ylänne 2009; Ehrlicher *et al.* 2011; Ruskamo *et al.* 2012; Rognoni *et al.* 2012). In contrast, the ligand-binding site of domain 17 is unmasked, and the function of the inter-domain interactions of domains 16–17 is unknown (Heikkinen *et al.* 2009). Domains 17, 19 and 21 belong to the same subgroup of β strand forming peptide-ligand binding domains, which are all able to bind the same ligands. Further, N-terminal domains 4, 9 and 12 belong in this subgroup (Ithychanda *et al.* 2009). To study whether similar inter-domain interactions exist in the N-terminal region of FLNs and whether they regulate ligand binding, the crystal structures of FLNa domains 3–5 and FLNc domains 4–5 were solved. The structures revealed a novel domain packing among an immunoglobulin-like domain family, which is conserved throughout the species and positively regulates ligand binding in domain 4.

I solved the structure of FLNa3–5, performed the respective SAXS analyses and conducted the sequence conservation analysis, which will be the focus of discussion in this and the following section.

FLNa domains 3–5 are packed side-by-side interacting along their β sheets and form a slightly bent triple sandwich structure (Fig. 11). The β sheets of each domain are aligned roughly parallel on top of each other with domain 3 slightly shifted so that the interaction between domains 3 and 4 is mediated only via the edges of one β strand of both domains. The A strand of domain 3 is faced

towards the G strand of domain 4 forming mostly polar interactions. The interaction between domains 4 and 5 is mediated by residues belonging to three β strands interacting on each side. The face formed by CFG strands of domain 4 forms a large hydrophobic interface around tryptophan 582 with the respective face of domain 5. The buried interface surface areas between the domains are approximately 500 Å^2 for domains 3–4 and 830 Å^2 for 4–5. Together, these results suggest that the interaction between domains 3 and 4 is significantly weaker than between domains 4 and 5. Simultaneously, my colleague Ritika Sethi solved the structure of FLNc4–5, which is largely identical to FLNa4–5 (root mean square deviation of 0.66 Å between 165 Cα atoms) with the key residues responsible for the interactions conserved (I, Fig. 2B and C).

The ligand-binding CD faces of the three domains are solvent exposed (Fig. 11). However, the CD faces of domains 3 and 5 are in a closed conformation as bending of the CD loop towards the C strand partially occludes the ligand binding interface. This suggests that domains 3 and 5 are unable to interact with the ligands through β sheet augmentation. Similar features can be seen in the structures of several other FLN immunoglobulin domains that do not interact with known β-strand-forming peptides (these include domains 10, 11, 13, 14, 15, 16, 18, 20 and 22, corresponding to PDB codes 2DIA, 2DIB, 2DJ4, 2E9J, 2DMB, 2EE9, 2DMC, 2D9I and 2D7B, respectively). Notably, FLNa5 is reported to interact with spleen tyrosine kinase (Falet *et al.* 2010); thus, the interaction between spleen tyrosine kinase and FLNa5 may represent a previously uncharacterised mechanism among FLN immunoglobulin-like domains.

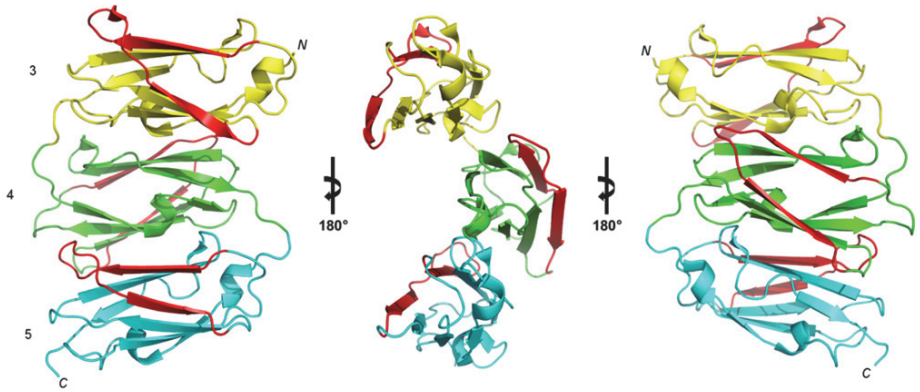

FIGURE 11 Crystal structure of FLNa3–5. The domains are packed side-by-side and form a bent triple sandwich structure. The CD faces (coloured red) are solvent exposed. Domain 3 is shown in yellow, 4 in green and 5 in cyan.

The observed domain packing is unique among the immunoglobulin superfamily and, therefore, several complementary techniques were used to confirm the interactions. First, the calculated x-ray scattering from the FLNa3–5 crystal structure was compared to experimental SAXS data. The structure was

in good agreement with the experimental SAXS data, rendering χ^2 value of 1.13, which indicates a very good fit (χ^2 reports the minimised discrepancy between the scattering profiles; Svergun *et al.* 1995). In addition, SAXS-derived *ab initio* shape envelope had high resemblance with the overall shape of the crystal structure. The *ab initio* shape envelope was aligned with the crystal structure with a normalised spatial discrepancy of 1.61 (I, Fig. 2E) (the normalised spatial discrepancy reports the minimised dissimilarity, being zero for identical objects; Kozin and Svergun 2001). Ritika Sethi verified the interaction by mutagenesis. Mutations of the interacting residues led to changes in SAXS parameters and loss of interaction between individual domains 4 and 5 in pull-down assays (I, Table II, Fig. 4A and B). Finally, Drs Helena Tossavainen and Perttu Permi performed ^{1}H-^{15}N HSQC chemical shift mapping between FLNc5 and FLNc4–5 to verify the interactions (I, Fig. 4C and D).

To discover, whether the observed novel domain packing is conserved throughout the animal kingdom, sequence alignment was performed using human FLNa/b/c3–5 and FLNa3–5 of *Mus musculus*, *Gallus gallus*, *Danio rerio* and *Drosophila melanogaster*. The sequence alignment (Fig. 12; I, Supplementary Fig. S1) showed that key residues at the inter-domain interfaces are largely conserved, suggesting that the observed domain packing is a general feature among FLNs in the animal kingdom and thus functionally important.

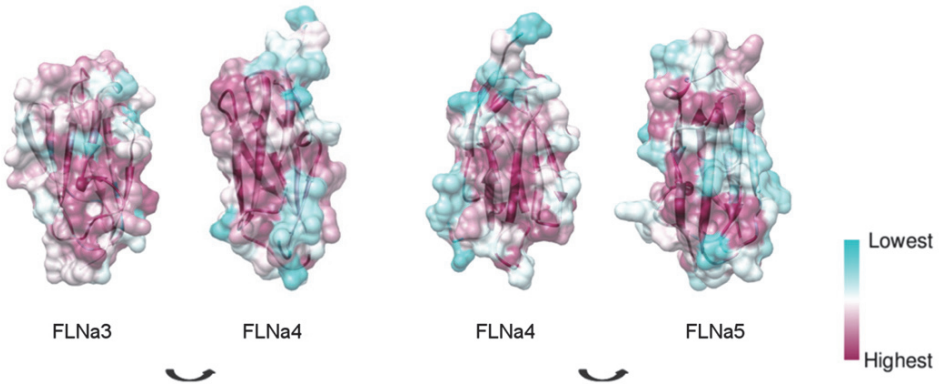

FIGURE 12 Surface residue conservation on the inter-domain interfaces of FLNa3–5. The key residues mediating the inter-domain interactions are largely conserved throughout the animal kingdom.

4.2 Domain 5 stabilises domain 4 that interacts with ligand peptides (I)

To investigate the function of the three-domain module, my colleague Ritika Sethi solved the structure of FLNc4–5 in complex with a peptide derived from glycoprotein Ibα (I, Fig. 6D), a receptor mediating platelet activation. The structure showed that domain 4 interacts with ligand peptides via the common

β sheet augmentation mechanism, as suggested by Ithychanda *et al*. (2009). The finding that the peptide interacted with domain 4 and not with the neighbouring domains is consistent with the closed conformation observed for domains 3 and 5. The thermal stability assay demonstrated that domain 5 stabilises domain 4 (I, Fig. 7). This suggests that in contrast to the rod 2 domain pairs that negatively regulate ligand binding, the inter-domain interactions of domain 4 and 5 might positively regulate ligand binding in domain 5. The function of the inter-domain interactions between domain 3 and 4, however, remain to be explained.

4.3 Ligand peptide-bound mechanosensory domain pair 20–21 is flexible but restricted in conformations (II)

During recent years, the mechanisms underlying the cellular mechanosensory function of FLNs have begun to emerge. It is evident that the two domain pairs 18–19 and 20–21, discussed in section 1.5.2, form the molecular basis for mechanosensing (Razinia *et al.* 2012). *In silico* and *in vitro* studies on FLNa20–21 show that the ligand-binding inhibitory A strand of domain 20 can be released by applying an external pulling force on the domain pair to promote ligand binding (Pentikäinen and Ylänne 2009; Ehrlicher *et al.* 2011; Rognoni *et al.* 2012). Recently, Nakamura et al. (2014) demonstrated that acto-myosin mediated contraction leads to changes in the domain organisation in cells. However, detailed structural level information on how the mechanosensory domain pairs are deformed upon ligand-binding is unclear. To study this, extensive structural studies, including SAXS measurements, crystallisation and NMR measurements with FLNa20–21 and migfilin-derived ligand-peptide were performed.

TABLE 2 SAXS-based structural parameters for FLNa20–21 and FLNaΔA20–21 in the absence and presence of migfilin peptide.

Sample	R_g (nm)[1]	D_{max} (nm)[2]
FLNa20–21	1.9	6.8
FLNa20–21+migfilin	2.3	8.2
FLNaΔA20–21	2.4	8.5
FLNaΔA20–21+migfilin	2.4	8.2

[1]Derived from the Guinier analysis. The error is ± 0.1 nm.
[2]Estimate from the pair-distance distribution calculation in program DATGNOM (Svergun *et al.*, 2001). The error is approximately 10%.

SAXS analysis demonstrated that FLNa20–21 forms a compact structure in solution that is extended upon peptide binding (II, Fig. 2). Peptide binding

induced a clear increase in radius of gyration, R_g, and a maximum dimension, D_{max}, of FLNa20–21 (Table 2). The conformational change was observed clearly from the pair-distance distribution function, *P(r),* that changed from a bell-shaped curve, typical for globular particles, into an asymmetric curve, typical for extended particles (Fig. 13).

As demonstrated in earlier studies, the observed changes are at least partially a result from the displacement of the A strand of FLNa20 (Pentikäinen *et al.* 2011; Ruskamo *et al.* 2012). Considering this, we performed the measurements with a domain pair lacking the inhibitory A strand, hereafter called FLNaΔA20–21. The data indicated that without the A strand of FLNa20, the domain pair is more elongated, and migfilin binding did not result in significant changes in the protein dimensions (Table 2 and Fig. 13A).

Next, dimensionless Kratky and Porod-Debye analyses of SAXS data were used to assess the conformational flexibility of the domain pair. In dimensionless Kratky, deviation from a bell-shaped curve indicates flexibility, whereas in a Porod-Debye plot, the loss of a clear plateau at low scatting angles tells the same (Rambo and Tainer 2011). The plots suggested that both migfilin binding (in the case of FLNa20-21) and removal of the A strand (in the case of FLNaΔA20–21) lead to increased flexibility of the domain pair. The peptide-bound profiles for both constructs were similar, whereas the non-ligated FLNa20-21 was significantly less flexible than FLNaΔA20–21 (Fig. 13B and C).

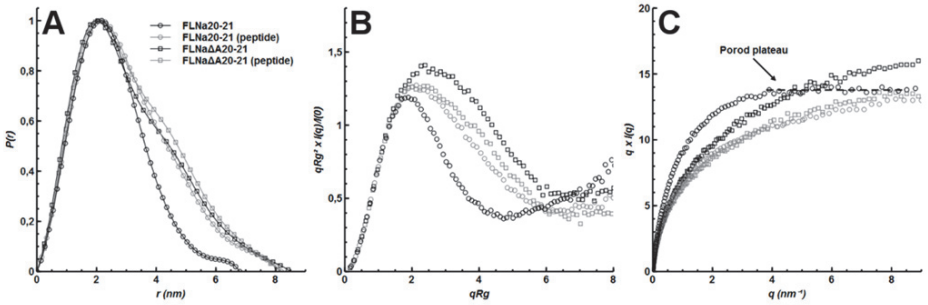

FIGURE 13 Model-independent analyses of SAXS data. (A) Pair-distance distribution function, (B) dimensionless-Kratky, and (C) Porod-Debye analyses for non-ligated and migfilin-peptide bound FLNa20–21 and FLNaΔA20–21.

To model the flexible peptide-bound structure of the domain pair in solution, ensemble optimization method (EOM) analysis was performed (Fig. 14). EOM allows an ensemble modelling of flexible macromolecules when suitable rigid body models are available (Bernado *et al.* 2007). The EOM analysis showed that FLNa20–21 is mostly compact with an average D_{max} (6.6 nm) comparable to those measured from the crystal structure. However, a minor population of extended conformations with an average D_{max} of 8.5 nm, in conjunction with the compact ones, fitted the scattering data and was selected by the EOM. The EOM selected models for the extended population suggest that the two domains are detached from each other. For peptide-bound FLNa20–21, the EOM selected

conformations with a wide size distribution very similar to the random models and had an average D_{max} of 7.5 nm. FLNaΔA20–21 differs from FLNa20–21. For FLNaΔA20–21, the EOM selected two populations of equal frequency with a D_{max} of 7.0 nm and 8.5 nm, respectively. The rigid body models suggest that the domains are separated in both populations. The peptide-bound distribution, however, is similar to that of FLNa20–21 with an average D_{max} of 7.5 nm.

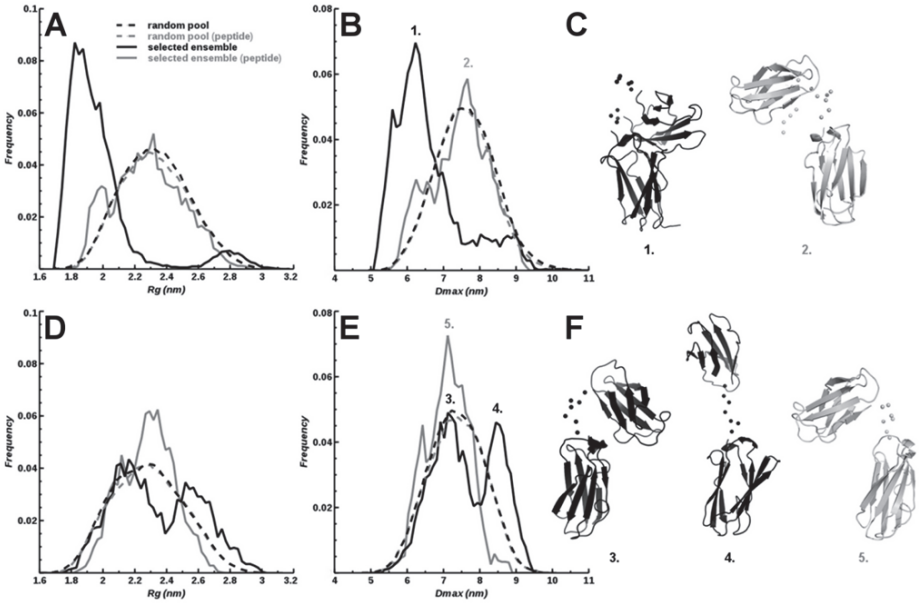

FIGURE 14 EOM analyses for FLNa20–21 (A–C) and FLNaΔA20–21 (D–F) with and without migfilin peptide. R_g (A,D) and D_{max} (B,E) distribution histograms for the random pool and selected ensembles. (C,F) EOM selected models corresponding to the most typical conformations (i.e. selected model having a D_{max} that roughly corresponds to the peak of the selected ensemble histograms).

These results are in agreement with the dimensionless Kratky and the Porod-Debye analyses discussed above. FLNa20–21 is compact, but the A strand deletion or peptide binding makes the domain pair flexible. Interestingly, the peptide-bound population falls between the compact and extended populations in terms of D_{max} observed without the peptide. The peptide seems to restrict the conformational space of the domain pair. The wide size distribution suggests larger conformational space and is in accordance with the increased flexibility upon peptide binding observed in the flexibility plots. This agrees with the flexibility plots and implies that the A strand of FLNa20 is important for the rigidity of the domain pair.

The crystal structure of FLNaΔA20–21 in complex with the migfilin peptide was solved to obtain detailed information on the conformational changes on the domain pair. The A strand deleted domain pair was used to avoid unstructured sequences that inhibit crystallisation. Residues 8–18 of the

peptide bind to the CD face of FLNa21, as reported by Lad *et al*. (2008). The two prolines at positions 19–20 bring structural rigidity to the peptide and bend it on top of domain 21, displacing domain 20 from its position in the FLNa19–21 crystal structure (Fig. 15). If the peptide from our current structure is placed in domain pair structure 20–21, the peptide causes a steric clash that would prevent domain 20 from interacting with domain 21. This would likely cause a conformational change leading to a lack of domain-domain interactions, as seen in the current structure.

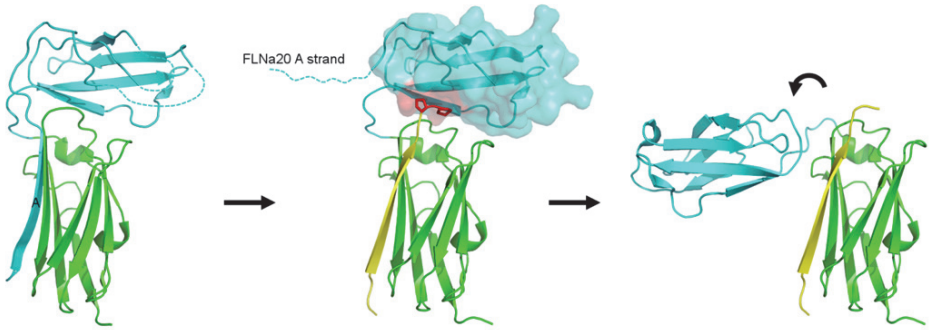

FIGURE 15 Migfilin peptide induced conformational change on FLNaΔA20–21 (FLNa ΔA20 in cyan and FLNa21 in green). On the left is the crystal structure of FLNa20–21 (from PDB code 2J3S). On the right is the peptide-bound crystal structure of the domain pair reported here. Migfilin peptide (in yellow) binding promotes a major conformational change to the domain pair. When the peptide is superimposed with the non-ligated domain pair structure (shown in the middle), the two consecutive prolines cause a steric clash with domain 20, presumably promoting the observed conformational change.

To gain more information about the flexibility of the peptide-bound domain pair in solution, NMR measurements with FLNaΔA20–21 were performed. These experiments were conducted by M.Sc. Nebojsa Rodic, Dr Helena Tossavainen and Dr Perttu Permi. The analysis was difficult because a major fraction of FLNaΔA20 HSQC peaks disappeared upon peptide addition. Consequently, changes at the inter–domain interface could not be mapped. However, the domain-level flexibility could be evaluated through ^{15}N T_1 and T_2 relaxation parameters. The parameters were significantly different between the individual domains and larger than those estimated from the molecular weight. Together, these suggested that the domains move partially independently of each other. The inter–domain loop restricts the movement of the domains, but allows some flexibility both in the absence and presence of the peptide (II, Supplementary Fig. S2). These observations agree with the SAXS analyses presented above and have been recorded earlier by Tossavainen *et al*. (2012) for full-length FLNa20–21 in assembly containing domains 16–21.

4.4 Three-conformational states model for domain pair 20–21 (II)

Together with the results presented above and reported earlier studies, a model of three-conformational states for FLNa20–21 can be proposed to explain the conformational changes on the domain pair (Fig. 16). These states are compact (i), open (ii) and ligand-bound (iii). The compact state represents the major population observed in the EOM analysis, when no ligand is present and is seen in crystal structure FLNa19–21. The compact state is in dynamic equilibrium with the open state, but when no force is applied, the compact state is favoured. These observations agree with recent single molecule force spectroscopy measurements. Small external forces – in a range capable of being produced by several myosin motors – shift the equilibrium towards the open state. However, extrapolation to zero force predicted that occasional opening of FLNa20 A strand can occur (Rognoni *et al.* 2012). In the open state, the domains are separated and can move rather freely via the inter–domain loop. Ligand binding to a compact or open state leads to the ligand-bound state (iii), characterised here. The ligand-bound state is less extended than the open one, and it is likely that the bound ligand restricts the mobility of the domains. In the crystal structure, the peptide was found to bend on top of domain 21 (Fig. 15). The following peptide residues presumably limit the movement of the inter–domain loop preventing the domain pair from adopting the open state. Peptide binding is reversible with dissociation constants in mM to μM range (Ithychanda *et al.* 2009).

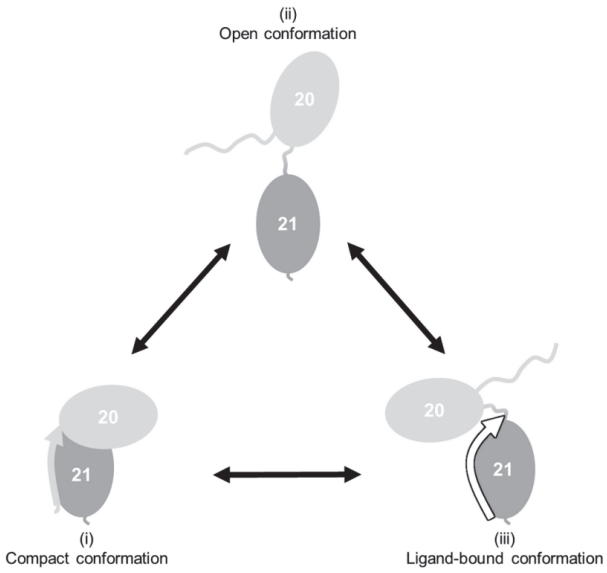

FIGURE 16 Three-conformational states model for FLNa20–21. The domain pair 20–21 adopts three conformations: compact (i) A strand bound, open (ii) A strand replaced and (iii) ligand-peptide bound conformations.

Closer inspection of previously solved complex structures of FLNa21 with different ligand-peptides revealed that all peptides have at least one proline and a bulky, charged amino acid following the residues responsible for the interaction with FLNa21 (II, Fig. 7) (Kiema *et al.* 2006; Nakamura *et al.* 2006; Takala *et al.* 2008; Smith *et al.* 2010). These structures suggest that all ligand-peptides could behave similarly and limit the flexibility of the inter–domain loop leading to peptide-bound conformation of the domain pair described above. Notably, FLNa18–19 is similar to FLNa20–21 in terms of the domain pair organisation, and domain 19 binds the same ligands as 21 (Heikkinen *et al.* 2009). Thus, it is possible that the model presented here also works for the FLNa18–19 domain pair.

To summarise, the data presented here shows that peptide-bound mechanosensory domain pair FLNa20–21 is flexible but restricted in conformational space because of steric effects caused by the migfilin peptide. This may also hold for other ligand-peptides and be important for the mechanosensory function of the domain pair.

4.5 Patient mutations lead to structural alterations in the domain pair 16–17 (III)

As mentioned by Heikkinen *et al*. (2009), the function of domain interactions between 16–17 is unknown. Three known missense mutations (L1788R in FLNa, G1834R, and S1902R in FLNb) leading to skeletal dysplasia on the domain pair have been found (Robertson *et al.* 2006; Daniel *et al.* 2012). Based on FLNa16–17 structure, they are all predicted to be located close to the inter-domain interface. As the molecular level mechanisms behind the disorders are imperfectly understood, these mutations were chosen for structural studies.

To gain detailed information on the position of the FLNb patient mutations G1834R and S1902R, FLNb16–17 was crystallised (Fig. 17). The A strand deleted protein was used because in FLNa16–17 (Heikkinen *et al.* 2009) and FLNb16 (PDB code 2EE9) NMR structures the A strand is unstructured. This unstructured segment might hamper the crystallisation. The structure was very similar to its FLNa counterpart (root mean square deviation of 0.96 for 145 Cα atoms). The residues at the inter-domain interface are conserved, except for two minor substitutions. The disease-causing patient mutations are located close to the inter-domain interface, G1834R at the A strand and S1902R at the G strand, as predicted.

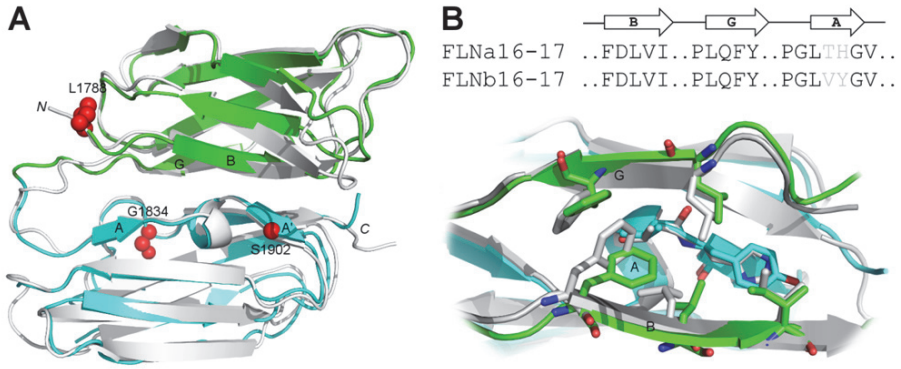

FIGURE 17 Crystal structure of FLNb16–17. (A) Structures of FLNa16–17 (in grey) and FLNb16–17 (FLNb16 in green and 17 in cyan) are superimposed. The location of the studied patient mutations are shown with red spheres. (B) Zoom-in to the key residues are responsible for the inter-domain interaction.

The effect of the mutations on the domain pair stability was first studied with the Thermofluor thermal stability assay (Pantoliano *et al.* 2001) (Fig. 18A–C). In this assay, the exposure of hydrophobic areas of the protein upon temperature induced unfolding is probed by a dye, which gives a fluorescent signal only when bound to a hydrophobic environment. Thus, well-folded proteins should have a low initial fluorescence signal, which rapidly increases upon melting transition and then decreases as a result of aggregation of the unfolded protein and thermal energy lowered affinity of the dye on the protein (Pantoliano *et al.* 2001). In Fig. 18, FLNa16 (in panel A) and FLNb17 (in panel B) show clearly interpretable melting curves. FLNb17 has a clear melting transition between 45–60 °C, after which the fluorescence decreases. As for FLNa16, the fluorescence intensity gradually increases until 65 °C followed by a sharp decrease. The respective domains, FLNa16 carrying L1788R mutation (in panel A) and FLNb17 carrying G1834R or S1902R mutation (in panel B), however, show a very high dye binding at ambient temperatures, suggesting that the proteins are not in their native state. A high initial fluorescence signal that decreases as a function of temperature is typical for an un- or misfolded protein, or, for instance, proteins with exposed hydrophobic patches (Pantoliano *et al.* 2001). For the two-domain fragments (Fig. 18C), FLNa16–17 showed a sharp melting transition between 53–63 °C. FLNb16–17 showed some ambient dye binding and a major melting transition between 60–70 °C. For FLNa16–17 L1788R mutation, the fluorescence increases steadily until 60 °C followed by a sharp decrease, as for single domain FLNa16. In contrast, FLNb16–17 mutants both show a typical curve for a poorly folded protein, as for the single mutant domains FLNb17. Altogether, all three mutants have an effect on the thermal stability of the protein, and the FLNb17 G1834R and S1902R mutations seem to destabilize the domain.

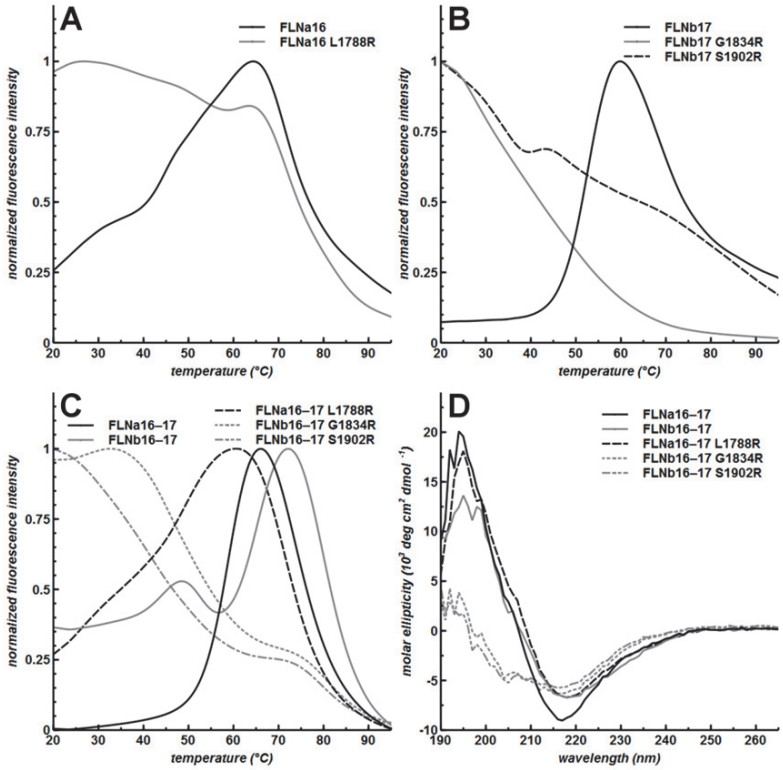

FIGURE 18 FLN16–17 patient mutations destabilise the domain pair. The thermal stability assay of wild type and mutated single domains (A–B) and domain pairs (C). (D) The circular dichroism spectra of the wild type and mutated domain pairs.

To further study the effect of the FLNa and FLNb mutations in the conformation of the domain pair, circular dichroism spectra were recorded for the purified two-domain fragments (Fig. 18D). Both FLNa16–17 and FLNb16–17 showed spectra typical for proteins with β sheet structure with a major positive peak in molar ellipticity at 195 nm and a major negative peak at 218 nm (Greenfield and Fasman 1969). The FLNa L1788R mutation caused no major alteration in the spectrum. However, both the FLNb G1834R and S1902R mutants showed altered spectra, suggesting major changes in the β sheet content.

Typically, poorly folded proteins are subjected to increased proteolysis in cells. The reduced stability caused by domain unfolding is known to lead to increased proteolysis of FLNc in myofibrillar myopathy (Vorgerd *et al.* 2005; Löwe *et al.* 2007; Kley *et al.* 2012). This may also be the case with the mutated FLN16–17. Domain 17 is also a known ligand-binding site (Nakamura *et al.* 2006; Ithychanda *et al.* 2009), and unfolding of the domain may prevent binding of currently unknown ligands that are important during bone morphogenesis, thereby affecting downstream signalling from the site.

The above results suggest that the patient mutations in FLNb17, G1834R and S1902R lead to drastic changes in domain stability and folding, whereas FLNa16 mutation L1788R seems to have less severe effects. To model the changes of this mutation on the domain pair, SAXS measurements were performed. The proteins behaved well and no severe aggregation or repulsion was detected. The L1788R mutation had a clear effect on the structural parameters of the domain pair (III, Table II). Next, *ab initio* shape envelopes for the wild type and L1788R domain pairs were generated (Fig. 19). All three models fitted well with the scattering data (chi values of 0.85–1.40) and the structures of the wild type domain pairs agreed with the respective globular shape envelopes (the normalised spatial discrepancy between structures and shape envelopes were 1.50–1.62) (III, Supplementary Fig. S2). Interestingly, the envelope of L1788R patient mutant was clearly extended in shape, suggesting an opening of the inter-domain interface (Fig. 19). This may have an influence on the possible force sensing of the domain pair, for instance, by revealing hidden uncharacterised binding sites. Stiffness sensing is a key process regulating bone morphogenesis and well documented in pathological mechanisms of many diseases (Orr *et al.* 2006). Further studies are required to study the cellular effects of the conformational change.

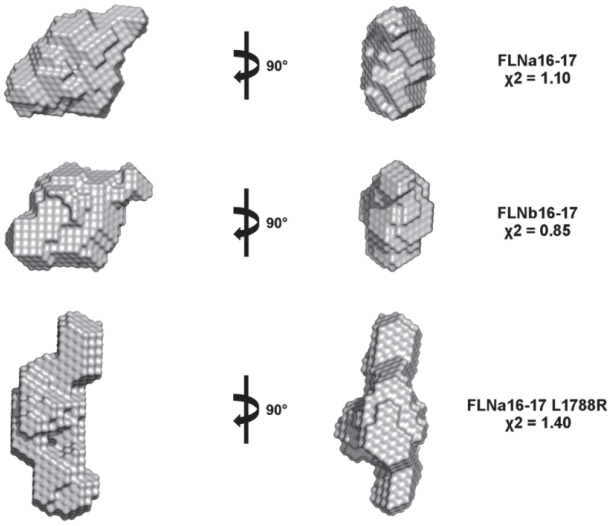

FIGURE 19 SAXS-derived *ab initio* shape envelopes for FLNa and b16–17 wild type and FLNa16–17 L1788R patient mutant.

5 CONCLUSIONS

The main conclusions of this thesis are as follows:

I Filamin domains 3–5 form a compact, partially flexible three-domain unit, whose packing is conserved throughout the animal kingdom. This kind of domain packing has not been observed earlier within the immunoglobulin superfamily. The common ligand-binding interfaces (CD faces) of domain 3 and 5 are in a conformation that may not be accessible for β sheet augmentation interactions. Instead, domain 5 stabilised domain 4, which is capable for such β strand forming interaction.

II The mechanosensory FLNa domain pair 20–21 has three distinct conformational states. The non-ligated domain pair forms a compact structure with occasional opening of the domain 20 A strand that masks the ligand-binding CD face of domain 21. This leads to an extended open conformation of the domain pair, where the domains can move rather freely with respect to each other. Migfilin peptide binding in domain 21 prevents interactions taking place between the domains. This is due to bending of the peptide on top of domain 21. In addition, the peptide likely restricts the movement of the inter-domain linker leading to reduced conformational freedom of the domains with respect to each other. Therefore, the migfilin peptide-bound structure of the domain pair is flexible but different in allowable conformations to a non-ligated A strand replaced open conformation. The represented model may be common to all ligand-peptides and also hold for the structurally similar domain pair 18–19.

III Skeletal dysplasia causing patient mutations in domain pair 16–17 destabilise the domain pair by either leading to domain 17 unfolding or opening of the inter-domain interface by causing other structural rearrangements in the domain. These may make the protein prone to increased proteolysis, alter ligand binding ability and change the mechanical signalling of the domain pair.

Acknowledgements

Now the work is done, it is time for my final words. The first words I dedicate to my great supervisors. I thank Jari Ylänne for giving me the opportunity to turn this card (and for drawing me from your deck of cards back then). You gave me the time and space to work independently, but were always available when needed, although sometimes very late in the afternoon. I enjoyed working with you over these years. Equally, I would like to thank Ulla Pentikäinen for all the help and discussions (both scientific and non-scientific) during these years. The beam line visits were especially fun, although 'sometimes things just plrrffffth'!

Tommi Kajander and Andrew Sutherland-Smith are acknowledged for the critical evaluation of this thesis and the excellent comments. Tommi, I would also like to thank you for the support and guidance over the years as my thesis committee member and the e-mail pre-defence.

Sanna, thank you for the friendship and peer support. We've had many joyful chat breaks during the work days and several fun moments outside the work environment. Let's continue (board) gaming in the future as well!

Miika, I thank you for the support during the writing of the thesis. You won the ridiculously timetabled race for the finish line by a hair's breadth. I have also enjoyed every jog and long lively discussions during these years. As said, we seemed to be on the same wavelength from the very first experiment.

Many thanks to my former and present group members: Ritika, Heikki, Nina, Lina, Tatu and Anita. You were all great colleagues. Lorenzo, Susanna and Ulla-Maria, your great contributions in the lab made it, in part, possible for me to finish in time – thank you. Allu, you deserve a special recognition for all the time saving tips you gave me in the lab and the countless high-quality protein preps you purified for me to work with.

Mikko, Lassi, Moona, Sanna R., Sakke, Dina, Piia, Matti, Kari and other colleagues from the department and ISB: thanks for all the evenings at the Nano sauna, the C2 corridor unisex toilet (exclusively Moona), the Lappish Karaoke bars and the often surprisingly cold saunas etc.

Special recognition goes to Faija and Mutsi for providing me the supporting and encouraging environment in which to grow up that has made this possible.

Finally, the warmest thanks go to Emmi for all your love, care and support. The work took a lot of time, energy and nerves, especially during the final months, but you were understanding, as always. Our steps increasingly agree as time goes by (although you still sometimes try to lead). I will make up all the lost moments, as I now have the long awaited 'half an hour time'.

YHTEENVETO (RÉSUMÉ IN FINNISH)

Rakennetutkimuksia filamiini-proteiinin domeenivuorovaikutuksilla

Monisoluisilla eliöillä solujen liikkuminen ja kiinnittyminen ympäristöönsä ovat välttämättömiä kudosten muodostumisen kannalta. Eläinsolujen liikkeen mahdollistaa säikeinen aktiinitukiranka, joka kasvaessaan työntää solukalvoa eteenpäin. Aktiinin toimintaa säätelevät lukuisat apuproteiinit. Filamiinit ovat yksi tällainen proteiiniperhe. Filamiinit ovat suurikokoisia proteiineja, jotka sitovat aktiinisäikeitä yhteen geelimäisiksi verkostoiksi solukalvon tuntumaan. Lisäksi ne toimivat kiinnittymisalustana toisille proteiineille ja osallistuvat tällä tavoin lukuisten solun toimintojen säätelyyn. Filamiinien monitahoisen toiminnan vuoksi ne ovat osallisina useissa perinnöllisissä sairauksissa, jotka aiheuttavat vakavia kehityshäiriöitä aivoihin, sydämeen, luustoon sekä lihaksiin.

Filamiinit koostuvat useasta rakenteellisesti itsenäisestä osasta, domeenista. Proteiiniketjun päässä on aktiinia sitova domeeni. Tähän on liittyneenä 24 immunoglobuliinin kaltaista domeenia, jotka toimivat proteiinivuorovaikutusten välikäsinä. Nämä domeenit muodostavat taipuisan sauvamaisen rakenteen. Osan domeeneista on havaittu vuorovaikuttavan keskenään ja muodostavan domeenipareja.

Erityisen mielenkiinnon kohteeksi filamiineissa on noussut niiden kyky toimia eräänlaisina voimamittareina. Solun normaalin kehityksen edellytyksenä on, että se aistii ympäristönsä mekaanisia ominaisuuksia. Tämän mahdollistavat proteiinit, jotka muuttavat muotoaan kohdatessaan mekaanisen ärsykkeen. Aikaisemmin on selvitetty, kuinka filamiinit aistivat niihin kohdistuvan ulkoisen rasituksen. Lepotilassa proteiinien sitoutumispaikka filamiinin domeeniparissa on peittyneenä, mutta se avautuu vetävän voiman vaikutuksesta ja mahdollistaa erityisten viestinvälittäjäproteiinien sitoutumisen.

Väitöskirjani tutkimuksissa keskityttiin filamiinidomeenien rakenteisiin. Pääasiallisina tutkimusmenetelminä käytettiin proteiinikristallografiaa sekä pienkulmaröntgensirontaa. Nämä menetelmät mahdollistavat proteiinien atomitason rakenteiden selvittämisen sekä proteiinivuorovaikutusten tutkimisen.

Ensimmäisessä osatyössä ratkaistiin uusi kolmen domeenin filamiinirakenne. Tämän kolmen domeenin yksikön osoitettiin olevan verihiutaleiden solukalvoproteiinin sitoutumispaikka. Rakenteessa havaitut domeenien väliset vuorovaikutukset vakauttavat solukalvoproteiinia sitovan keskimmäisen domeenin. Onkin mahdollista, että filamiiniin kohdistuvan vetävän voiman vaikutuksesta domeenien väliset vuorovaikutukset purkautuvat ja solukalvoproteiinin sitoutuminen estyy. Tämä olisi uusi mekanismi, jolla filamiinit säätelevät proteiinivuorovaikutuksia ulkoisen voiman vaikutuksesta.

Toisessa osatyössä tarkasteltiin voimamittarina toimivassa domeeniparissa tapahtuvia rakenteellisia muutoksia solujen tarttumista säätelevän proteiinin sitoutuessa pariin. Tutkimuksessa havaittiin, että säätelyproteiinin sitoutuessa domeeniparin vuorovaikutukset purkautuvat. Domeeniparista tulee rakenteeltaan joustava, mutta sitoutunut säätelyproteiini rajoittaa domeenien liikettä ja

lukitsee ne liikkumaan tietyissä kulmissa toisiinsa nähden. Tämä rakennemuutos saattaa olla tärkeä säätelymekanismi voimamittarin toiminnassa.

Viimeisessä osatyössä tutkittiin luuston kehityshäiriöihin johtavien mutaatioiden rakenteellisia vaikutuksia aikaisemmin löydettyyn filamiinin domeeniparii, jonka toiminta solussa on epäselvä. Tutkimuksessa todettiin, että mutaatiot joko johtavat domeenirakenteen hajoamiseen tai muuttavat domeeniparin välisiä vuorovaikutuksia mahdollisesti irrottaen domeenit toisistaan. Rakenteen purkautuminen saattaa estää luiden kehityksen kannalta tärkeän viestinvälittäjäproteiinin sitoutumisen domeeniparii sekä johtaa filamiinin ennenaikaiseen pilkkomiseen soluissa. Domeeniparin avautuminen puolestaan saattaa paljastaa aiemmin tuntemattoman proteiinin sitoutumispaikan parissa ja lisätä siten filamiinin aktiivisuutta.

Väitöskirja tuo uutta tietoa filamiinien rakenteista ja toiminnasta voimamittareina sekä paljastaa syitä filamiinien rakenteen ja toiminnan muutoksista vakavien luuston kehityshäiriöiden taustalla.

REFERENCES

Bernado P., Mylonas E., Petoukhov M. V, Blackledge M. & Svergun D.I. 2007. Structural characterization of flexible proteins using small-angle X-ray scattering. *J. Am. Chem. Soc.* 129: 5656–5664.

Bicknell L.S., Morgan T., Bonafé L., Wessels M.W., Bialer M.G., Willems P.J., Cohn D.H., Krakow D. & Robertson S.P. 2005. Mutations in FLNB cause boomerang dysplasia. *J. Med. Genet.* 42: e43.

Bresnick A.R., Janmey P. & Condeelis J. 1991. Evidence that a 27-residue sequence is the actin-binding site of ABP-120. *J. Biol. Chem.* 266: 12989–12993.

Clark A.R., Sawyer G.M., Robertson S.P. & Sutherland-Smith A.J. 2009. Skeletal dysplasias due to filamin A mutations result from a gain-of-function mechanism distinct from allelic neurological disorders. *Hum. Mol. Genet.* 18: 4791–4800.

Daniel P.B., Morgan T., Alanay Y., Bijlsma E., Cho T.-J., Cole T., Collins F., David A., Devriendt K., Faivre L., Ikegawa S., Jacquemont S., Jesic M., Krakow D., Liebrecht D., Maitz S., Marlin S., Morin G., Nishikubo T., Nishimura G., Prescott T., Scarano G., Shafeghati Y., Skovby F., Tsutsumi S., Whiteford M., Zenker M. & Robertson S.P. 2012. Disease-associated mutations in the actin-binding domain of filamin B cause cytoplasmic focal accumulations correlating with disease severity. *Hum. Mutat.* 33: 665–673.

Duff R.M., Tay V., Hackman P., Ravenscroft G., McLean C., Kennedy P., Steinbach A., Schöffler W., Ven P.F.M. Van Der, Fürst D.O., Song J., Djinović-Carugo K., Penttilä S., Raheem O., Reardon K., Malandrini A., Gambelli S., Villanova M., Nowak K.J., Williams D.R., Landers J.E., Brown R.H., Udd B. & Laing N.G. 2011. Mutations in the N-terminal actin-binding domain of filamin C cause a distal myopathy. *Am. J. Hum. Genet.* 88: 729–740.

Duval D., Lardeux A., Tourneau T. Le, Norris R.A., Markwald R.R., Sauzeau V., Probst V., Marec H. Le, Levine R., Schott J.J. & Merot J. 2014. Valvular dystrophy associated filamin A mutations reveal a new role of its first repeats in small-GTPase regulation. *Biochim. Biophys. Acta* 1843: 234–244.

Ehrlicher J., Nakamura F., Hartwig J.H., Weitz D. & Stossel T.P. 2011. Mechanical strain in actin networks regulates FilGAP and integrin binding to filamin A. *Nature* 478: 260–263.

Engler A.J., Sen S., Sweeney H.L. & Discher D.E. 2006. Matrix Elasticity Directs Stem Cell Lineage Specification. *Cell* 126: 677–689.

Falet H., Pollitt A.Y., Begonja A.J., Weber S.E., Duerschmied D., Wagner D.D., Watson S.P. & Hartwig J.H. 2010. A novel interaction between FlnA and Syk regulates platelet ITAM-mediated receptor signaling and function. *J. Exp. Med.* 207: 1967–1979.

Flier A. Van Der, Kuikman I., Kramer D., Geerts D., Kreft M., Takafuta T., Shapiro S.S. & Sonnenberg A. 2002. Different splice variants of filamin-B

affect myogenesis, subcellular distribution, and determine binding to integrin [beta] subunits. *J. Cell Biol.* 156: 361–376.

Flier A. Van Der & Sonnenberg A. 2001. Structural and functional aspects of filamins. *Biochim. Biophys. Acta* 1538: 99–117.

Fox J.W., Lamperti E.D., Ekşioğlu Y.Z., Hong S.E., Feng Y., Graham D., Scheffer I.E., Dobyns W.B., Hirsch B., Radtke R., Berkovic S.F., Huttenlocher P.R. & Walsh C. 1998. Mutations in filamin 1 prevent migration of cerebral cortical neurons in human periventricular heterotopia. *Neuron* 21: 1315–1325.

Franzot G., Sjöblom B., Gautel M. & Carugo K.D. 2005. The crystal structure of the actin binding domain from α-actinin in its closed conformation: Structural insight into phospholipid regulation of α-actinin. *J. Mol. Biol.* 348: 151–165.

Fritz-Laylin L.K., Prochnik S.E., Ginger M.L., Dacks J.B., Carpenter M.L., Field M.C., Kuo A., Paredez A., Chapman J., Pham J., Shu S., Neupane R., Cipriano M., Mancuso J., Tu H., Salamov A., Lindquist E., Shapiro H., Lucas S., Grigoriev I. V., Cande W.Z., Fulton C., Rokhsar D.S. & Dawson S.C. 2010. The Genome of *Naegleria gruberi* Illuminates Early Eukaryotic Versatility. *Cell* 140: 631–642.

Fucini P., Renner C., Herberhold C., Noegel A. & Holak T. 1997. The repeating segments of the F-actin cross-linking gelation factor (ABP-120) have an immunoglobulin-like fold. *Nat. Struct. Biol.* 4: 223–230.

Furuike S., Ito T. & Yamazaki M. 2001. Mechanical unfolding of single filamin A (ABP-280) molecules detected by atomic force microscopy. *FEBS Lett.* 498: 72–75.

Fürst D.O., Goldfarb L.G., Kley R., Vorgerd M., Olivé M. & Ven P.F.M. Van Der. 2013. Filamin C-related myopathies: Pathology and mechanisms. *Acta Neuropathol.* 125: 33–46.

García-Alvarez B., Bobkov A., Sonnenberg A. & Pereda J.M. De. 2003. Structural and functional analysis of the actin binding domain of plectin suggests alternative mechanisms for binding to F-actin and integrin β4. *Structure* 11: 615–625.

Gardel M.L., Nakamura F., Hartwig J.H., Crocker J.C., Stossel T.P. & Weitz D. 2006. Prestressed F-actin networks cross-linked by hinged filamins replicate mechanical properties of cells. *Proc. Natl. Acad. Sci. U. S. A.* 103: 1762–1767.

Gehler S., Baldassarre M., Lad Y., Leight J.L., Wozniak M.A., Riching K.M., Eliceiri K.W., Weaver V.M., Calderwood D.A. & Keely P.J. 2009. Filamin A-beta1 integrin complex tunes epithelial cell response to matrix tension. *Mol. Biol. Cell* 20: 3224–3238.

Gimona M., Djinovic-Carugo K., Kranewitter W.J. & Winder S.J. 2002. Functional plasticity of CH domains. *FEBS Lett.* 513: 98–106.

Glogauer M., Arora P., Chou D., Janmey P., Downey G.P. & McCulloch C. G. 1998. The role of actin-binding protein 280 in integrin-dependent mechanoprotection. *J. Biol. Chem.* 273: 1689–1698.

Gorlin J.B., Yamin R., Egan S., Stewart M., Stossel T.P., Kwiatkowski D.J. & Hartwig J.H. 1990. Human endothelial actin-binding protein (ABP-280, nonmuscle filamin): a molecular leaf spring. *J. Cell Biol.* 111: 1089–1105.

Greenfield N. & Fasman G.D. 1969. Computed circular dichroism spectra for the evaluation of protein conformation. *Biochemistry* 8: 4108–4116.

Hartwig J.H. & Stossel T.P. 1975. Isolation and properties of actin, myosin, and a new actin binding protein in rabbit alveolar macrophages. *J. Biol. Chem.* 250: 5696–5705.

Heikkinen O.K., Ruskamo S., Konarev P. V, Svergun D.I., Iivanainen T., Heikkinen S.M., Permi P., Koskela H., Kilpeläinen I. & Ylänne J. 2009. Atomic structures of two novel immunoglobulin-like domain pairs in the actin cross-linking protein filamin. *J. Biol. Chem.* 284: 25450–25458.

Hemmings L., Kuhlman P. & Critchley D.R. 1992. Analysis of the actin-binding domain of α-actinin by mutagenesis and demonstration that dystrophin contains a functionally homologous domain. *J. Cell Biol.* 116: 1369–1380.

Himmel M., Ven P.F.M. Van der, Stöcklein W. & Fürst D.O. 2003. The limits of promiscuity: Isoform-specific dimerization of filamins. *Biochemistry* 42: 430–439.

Hock R.S. & Condeelis J.S. 1987. Isolation of a 240-kilodalton actin-binding protein from *Dictyostelium disoideum*. *J. Biol. Chem.* 262: 394–400.

Ithychanda S.S., Hsu D., Li H., Yan L., Liu D.D., Liu D., Das M., Plow E.F. & Qin J. 2009. Identification and characterization of multiple similar ligand-binding repeats in filamin: implication on filamin-mediated receptor clustering and cross-talk. *J. Biol. Chem.* 284: 35113–35121.

Kainulainen T., Pender A., D'Addario M., Feng Y., Lekic P. & McCulloch C. 2002. Cell death and mechanoprotection by filamin A in connective tissues after challenge by applied tensile forces. *J. Biol. Chem.* 277: 21998–22009.

Kiema T., Lad Y., Jiang P., Oxley C.L., Baldassarre M., Wegener K.L., Campbell I.D., Ylänne J. & Calderwood D. 2006. The molecular basis of filamin binding to integrins and competition with talin. *Mol. Cell* 21: 337–347.

Klein M.G., Shi W., Ramagopal U., Tseng Y., Wirtz D., Kovar D.R., Staiger C.J. & Almo S.C. 2004. Structure of the actin crosslinking core of fimbrin. *Structure* 12: 999–1013.

Kley R., Serdaroglu-Oflazer P., Leber Y., Odgerel Z., Ven P.F.M. Van Der, Olivé M., Ferrer I., Onipe A., Mihaylov M., Bilbao J.M., Lee H.S., Höhfeld J., Djinović-Carugo K., Kong K., Tegenthoff M., Peters S., Stenzel W., Vorgerd M., Goldfarb L.G. & Fürst D.O. 2012. Pathophysiology of protein aggregation and extended phenotyping in filaminopathy. *Brain* 135: 2642–2660.

Kogelenberg M. van, Clark A.R., Jenkins Z., Morgan T., Anandan A., Sawyer G.M., Edwards M., Dudding T., Homfray T., Castle B., Tolmie J., Stewart F., Kivuva E., Pilz D.T., Gabbett M., Sutherland-Smith A.J. & Robertson S.P. 2015. Diverse phenotypic consequences of mutations affecting the C-terminus of FLNA. *J. Mol. Med.*

Kolahi K.S. & Mofrad M.R.K. 2008. Molecular mechanics of filamin's rod domain. *Biophys. J.* 94: 1075–1083.

Kozin M.B. & Svergun D.I. 2001. Automated matching of high- and low-resolution structural models. *J. Appl. Crystallogr.* 34: 33–41.

Krakow D., Robertson S.P., King L.M., Morgan T., Sebald E.T., Bertolotto C., Wachsmann-Hogiu S., Acuna D., Shapiro S.S., Takafuta T., Aftimos S., Kim C.A., Firth H., Steiner C.E., Cormier-Daire V., Superti-Furga A., Bonafe L., Graham J.M., Grix A., Bacino C., Allanson J., Bialer M.G., Lachman R.S., Rimoin D.L. & Cohn D.H. 2004. Mutations in the gene encoding filamin B disrupt vertebral segmentation, joint formation and skeletogenesis. *Nat. Genet.* 36: 405–410.

Kuhlman P., Hemmings L. & Critchley D.R. 1992. The identification and characterisation of an actin-binding site in alpha-actinin by mutagenesis. *FEBS Lett.* 304: 201–206.

Kyndt F., Gueffet J.P., Probst V., Jaafar P., Legendre A., Bouffant F. Le, Toquet C., Roy E., McGregor L., Lynch S.A., Newbury-Ecob R., Tran V., Young I., Trochu J.N., Marec H. Le & Schott J.J. 2007. Mutations in the gene encoding filamin A as a cause for familial cardiac valvular dystrophy. *Circulation* 115: 40–49.

Lad Y., Jiang P., Ruskamo S., Harburger D.S., Ylänne J., Campbell I.D. & Calderwood D. 2008. Structural basis of the migfilin-filamin interaction and competition with integrin beta tails. *J. Biol. Chem.* 283: 35154–35163.

Lad Y., Kiema T., Jiang P., Pentikäinen O.T., Coles C.H., Campbell I.D., Calderwood D. & Ylänne J. 2007. Structure of three tandem filamin domains reveals auto-inhibition of ligand binding. *EMBO J.* 26: 3993–4004.

Lamsoul I., Burande C.F., Razinia Z., Houles T.C., Menoret D., Baldassarre M., Erard M., Moog-Lutz C., Calderwood D. & Lutz P.G. 2011. Functional and structural insights into ASB2α, a novel regulator of integrin-dependent adhesion of hematopoietic cells. *J. Biol. Chem.* 286: 30571–30581.

Langer L.O., Gorlin R.J., Donnai D., Hamel B.C. & Clericuzio C. 1994. Spondylocarpotarsal synostosis syndrome (with or without unilateral unsegmented bar). *Am. J. Med. Genet.* 51: 1–8.

Li C., Yu S., Nakamura F., Pentikäinen O.T., Singh N., Yin S., Xin W. & Sy M.S. 2010. Pro-prion binds filamin A, facilitating its interaction with integrin β1, and contributes to melanomagenesis. *J. Biol. Chem.* 285: 30328–30339.

Light S., Sagit R., Ithychanda S.S., Qin J. & Elofsson A. 2012. The evolution of filamin - A protein domain repeat perspective. *J. Struct. Biol.* 179: 289–298.

Löwe T., Kley R., Ven P.F.M. Van der, Himmel M., Huebner A., Vorgerd M. & Fürst D.O. 2007. The pathomechanism of filaminopathy: Altered biochemical properties explain the cellular phenotype of a protein aggregation myopathy. *Hum. Mol. Genet.* 16: 1351–1358.

Maestrini E., Patrosso C., Mancini M., Rivella S., Rocchi M., Repetto M., Villa A., Frattini A., Zoppe M., Vezzoni P. & et al. 1993. Mapping of two genes encoding isoforms of the actin binding protein ABP- 280, a dystrophin like protein, to Xq28 and to chromosome 7. *Hum. Mol. Genet.* 2: 761–766.

Martinac B. 2004. Mechanosensitive ion channels: molecules of mechanotransduction. *J. Cell Sci.* 117: 2449–2460.

Nakamura F., Heikkinen O., Pentikäinen O.T., Osborn T.M., Kasza K.E., Weitz D., Kupiainen O., Permi P., Kilpeläinen I., Ylänne J., Hartwig J.H. & Stossel T.P. 2009. Molecular basis of filamin A-FilGAP interaction and its impairment in congenital disorders associated with filamin A mutations. *PloS One* 4: e4928.

Nakamura F., Osborn T.M., Hartemink C., Hartwig J.H. & Stossel T.P. 2007. Structural basis of filamin A functions. *J. Cell Biol.* 179: 1011–1025.

Nakamura F., Pudas R., Heikkinen O., Permi P., Kilpeläinen I., Munday A.D., Hartwig J.H., Stossel T.P. & Ylänne J. 2006. The structure of the GPIb-filamin A complex. *Blood* 107: 1925–1932.

Nakamura F., Song M., Hartwig J.H. & Stossel T.P. 2014. Documentation and localization of force-mediated filamin A domain perturbations in moving cells. *Nat. Commun.* 5: 4656.

Nakamura F., Stossel T.P. & Hartwig J.H. 2011. The filamins: Organizers of cell structure and function. *Cell Adh. Migr.* 5: 160–169.

Orr W., Helmke B.P., Blackman B.R. & Schwartz M. 2006. Mechanisms of mechanotransduction. *Dev. Cell* 10: 11–20.

Pantoliano M.W., Petrella E.C., Kwasnoski J.D., Lobanov V.S., Myslik J., Graf E., Carver T., Asel E., Springer B., Lane P. & Salemme F.R. 2001. High-density miniaturized thermal shift assays as a general strategy for drug discovery. *J. Biomol. Screen.* 6: 429–440.

Parrini E., Ramazzotti A., Dobyns W.B., Mei D., Moro F., Veggiotti P., Marini C., Brilstra E.H., Bernardina B.D., Goodwin L., Bodell A., Jones M.C., Nangeroni M., Palmeri S., Said E., Sander J.W., Striano P., Takahashi Y., Maldergem L. Van, Leonardi G., Wright M., Walsh C. & Guerrini R. 2006. Periventricular heterotopia: Phenotypic heterogeneity and correlation with Filamin a mutations. *Brain* 129: 1892–1906.

Pentikäinen U., Jiang P., Takala H., Ruskamo S., Campbell I.D. & Ylänne J. 2011. Assembly of a filamin four-domain fragment and the influence of splicing variant-1 on the structure. *J. Biol. Chem.* 286: 26921–26930.

Pentikäinen U. & Ylänne J. 2009. The regulation mechanism for the auto-inhibition of binding of human filamin A to integrin. *J. Mol. Biol.* 393: 644–657.

Pinto V.I., Senini V.W., Wang Y., Kazembe M.P. & McCulloch C. 2014. Filamin A protects cells against force-induced apoptosis by stabilizing talin- and vinculin-containing cell adhesions. *FASEB J.* 28: 453–463.

Pudas R., Kiema T.-R., Butler P.J.G., Stewart M. & Ylänne J. 2005. Structural Basis for Vertebrate Filamin Dimerization. *Structure* 13: 111–119.

Rambo R.P. & Tainer J. 2011. Characterizing flexible and intrinsically unstructured biological macromolecules by SAS using the Porod-Debye law. *Biopolymers* 95: 559–571.

Razinia Z., Mäkelä T., Ylänne J. & Calderwood D. 2012. Filamins in mechanosensing and signaling. *Annu. Rev. Biophys.* 41: 227–246.

Robertson S.P. 2007. Otopalatodigital syndrome spectrum disorders: otopalatodigital syndrome types 1 and 2, frontometaphyseal dysplasia and Melnick-Needles syndrome. *Eur. J. Hum. Genet.* 15: 3–9.

Robertson S.P. & Daniel P.B. 2012. Filamins and Disease. In: Kavallaris M. (ed.). *Cytoskeleton and Human Disease*, Humana Press. pp 141–158.

Robertson S.P., Jenkins Z.A., Morgan T., Adès L., Aftimos S., Boute O., Fiskerstrand T., Garcia-Miñaur S., Grix A., Green A., Kaloustian V. Der, Lewkonia R., McInnes B., Haelst M.M. Van, Macini G., Ilés T., Mortier G., Newbury-Ecob R., Nicholson L., Scott C.I., Ochman C., Brozek I., Shears D.J., Superti-Furga A., Suri M., Whiteford M., Wilkie A.O.M. & Krakows D. 2006. Frontometaphyseal dysplasia: Mutations in FLNA and phenotypic diversity. *Am. J. Med. Genet. Part A* 140: 1726–1736.

Robertson S.P., Twigg S.R.F., Sutherland-Smith A.J., Biancalana V., Gorlin R.J., Horn D., Kenwrick S.J., Kim C., Morava E., Newbury-Ecob R., Orstavik K.H., Quarrell O.W.J., Schwartz C.E., Shears D.J., Suri M., Kendrick-Jones J. & Wilkie A.O.M. 2003. Localized mutations in the gene encoding the cytoskeletal protein filamin A cause diverse malformations in humans. *Nat. Genet.* 33: 487–491.

Rognoni L., Stigler J., Pelz B., Ylänne J. & Rief M. 2012. Dynamic force sensing of filamin revealed in single-molecule experiments. *Proc. Natl. Acad. Sci. U. S. A.* 109: 19679–19684.

Ruskamo S., Gilbert R., Hofmann G., Jiang P., Campbell I.D., Ylänne J. & Pentikäinen U. 2012. The C-terminal rod 2 fragment of filamin A forms a compact structure that can be extended. *Biochem. J.* 446: 261–269.

Ruskamo S. & Ylänne J. 2009. Structure of the human filamin A actin-binding domain. *Acta Crystallogr. D. Biol. Crystallogr.* 65: 1217–1221.

Sawyer G.M., Clark A.R., Robertson S.P. & Sutherland-Smith A.J. 2009. Disease-associated Substitutions in the Filamin B Actin Binding Domain Confer Enhanced Actin Binding Affinity in the Absence of Major Structural Disturbance: Insights from the Crystal Structures of Filamin B Actin Binding Domains. *J. Mol. Biol.* 390: 1030–1047.

Sawyer G.M. & Sutherland-Smith A.J. 2012. Crystal structure of the filamin N-terminal region reveals a hinge between the actin binding and first repeat domains. *J. Mol. Biol.* 424: 240–247.

Seo M.-D., Seok S.-H., Im H., Kwon A.-R., Lee S.J., Kim H.-R., Cho Y., Park D. & Lee B.-J. 2009. Crystal structure of the dimerization domain of human filamin A. *Proteins* 75: 258–263.

Sethi R. & Ylänne J. 2014. Small-Angle X-Ray Scattering Reveals Compact Domain-Domain Interactions in the N-Terminal Region of Filamin C. *PloS One* 9: e107457.

Sheen V.L., Feng Y., Graham D., Takafuta T., Shapiro S.S. & Walsh C. 2002. Filamin A and Filamin B are co-expressed within neurons during periods of neuronal migration and can physically interact. *Hum. Mol. Genet.* 11: 2845–2854.

Smith L., Page R.C., Xu Z., Kohli E., Litman P., Nix J.C., Ithychanda S.S., Liu J., Qin J., Misra S. & Liedtke C.M. 2010. Biochemical basis of the interaction between cystic fibrosis transmembrane conductance regulator and immunoglobulin-like repeats of filamin. *J. Biol. Chem.* 285: 17166–17176.

Sokol N.S. & Cooley L. 1999. *Drosophila* filamin encoded by the cheerio locus is a component of ovarian ring canals. *Curr. Biol.* 9: 1221–1230.

Sutherland-Smith A.J. 2011. Filamin structure, function and mechanics: are altered filamin-mediated force responses associated with human disease? *Biophys. Rev.* 3: 15–23.

Svergun D., Barberato C. & Koch M.H. 1995. CRYSOL - A program to evaluate X-ray solution scattering of biological macromolecules from atomic coordinates. *J. Appl. Crystallogr.* 28: 768–773.

Svergun D.I., Petoukhov M. V & Koch M.H. 2001. Determination of domain structure of proteins from X-ray solution scattering. *Biophys. J.* 80: 2946–2953.

Takafuta T., Wu G., Murphy G.F. & Shapiro S.S. 1998. Human beta-filamin is a new protein that interacts with the cytoplasmic tail of glycoprotein Ib alpha. *J. Biol. Chem.* 273: 17531–17538.

Takala H., Nurminen E., Nurmi S.M., Aatonen M., Strandin T., Takatalo M., Kiema T., Gahmberg C.G., Ylänne J. & Fagerholm S.C. 2008. Beta2 integrin phosphorylation on Thr758 acts as a molecular switch to regulate 14-3-3 and filamin binding. *Blood* 112: 1853–1862.

Tossavainen H., Koskela O., Jiang P., Ylänne J., Campbell I.D., Kilpeläinen I. & Permi P. 2012. Model of a six immunoglobulin-like domain fragment of filamin A (16-21) built using residual dipolar couplings. *J Am Chem Soc.* 134: 6660–6672.

Wang K., Ash J.F. & Singer S.J. 1975. Filamin, a new high-molecular-weight protein found in smooth muscle and non-muscle cells. *Proc. Natl. Acad. Sci. U. S. A.* 72: 4483–4486.

Vargas M., Sansonetti P. & Guillén N. 1996. Identification and cellular localization of the actin-binding protein ABP-120 from *Entamoeba histolytica*. *Mol. Microbiol.* 22: 849–857.

Ven P.F.M. Van Der, Obermann W.M.J., Lemke B., Gautel M., Weber K. & Fürst D.O. 2000. Characterization of muscle filamin isoforms suggests a possible role of γ-Filamin/ABP-L in sarcomeric Z-disc formation. *Cell Motil. Cytoskeleton* 45: 149–162.

Wilson R., Ainscough R., Anderson K., Baynes C., Berks M., Bonfield J., Burton J., Connell M., Copsey T. & Cooper J. 1994. 2.2 Mb of contiguous nucleotide sequence from chromosome III of *C. elegans*. *Nature* 368: 32–38.

Vogel C., Bashton M., Kerrison N.D., Chothia C. & Teichmann S. 2004. Structure, function and evolution of multidomain proteins. *Curr. Opin. Struct. Biol.* 14: 208–216.

Vogel V. & Sheetz M. 2006. Local force and geometry sensing regulate cell functions. *Nat. Rev. Mol. Cell Biol.* 7: 265–275.

Vorgerd M., Ven P.F.M. van der, Bruchertseifer V., Löwe T., Kley R., Schröder R., Lochmüller H., Himmel M., Koehler K., Fürst D.O. & Huebner A. 2005. A mutation in the dimerization domain of filamin c causes a novel type of autosomal dominant myofibrillar myopathy. *Am. J. Hum. Genet.* 77: 297–304.

Xie Z., Xu W., Davie E.W. & Chung D.W. 1998. Molecular cloning of human ABPL, an actin-binding protein homologue. *Biochem. Biophys. Res. Commun.* 251: 914–919.

Yamazaki M., Furuike S. & Ito T. 2002. Mechanical response of single filamin A (ABP-280) molecules and its role in the actin cytoskeleton. *J. Muscle Res. Cell Motil.* 23: 525–534.

Zhou A.-X., Hartwig J.H. & Akyürek L.M. 2010. Filamins in cell signaling, transcription and organ development. *Trends Cell Biol.* 20: 113–123.

ORIGINAL PAPERS

I

A NOVEL STRUCTURAL UNIT IN THE N-TERMINAL REGION OF FILAMINS

by

Ritika Sethi, Jonne Seppälä, Helena Tossavainen, Mikko Ylilauri, Salla Ruskamo, Olli T. Pentikäinen, Ulla Pentikäinen, Perttu Permi, and Jari Ylänne

2014

Journal of Biological Chemistry, 289: 8588–8598.

A Novel Structural Unit in the N-Terminal Region of Filamins*

Ritika Sethi[1], Jonne Seppälä[1], Helena Tossavainen[2], Mikko Ylilauri[1], Salla Ruskamo[3], Olli T. Pentikäinen[1], Ulla Pentikäinen[1], Perttu Permi[2], and Jari Ylänne[1]

[1]From the Department of Biological and Environmental Science and Nanoscience Center, University of Jyväskylä, P.O Box 35, Survontie 9, 40014 Jyväskylä, Finland

[2] Program in Structural Biology and Biophysics, Institute of Biotechnology, University of Helsinki, FI-00014, Helsinki, Finland

[3] Department of Biochemistry and Biocenter Oulu, University of Oulu, P.O Box 3000, 90014 Oulu, Finland

*Running Title: *Structures and interactions of Filamin domains 3, 4 and 5*

To whom correspondence should be addressed: Jari Ylänne or Ritika Sethi, Department of Biological and Environmental Science and Nanoscience Center, University of Jyväskylä, P.O Box 35, Survontie 9, 40014 Jyväskylä, Finland, fax +35814617 239, telephone: +358504285273 (JY), +358440777438 (RS); Email: jari.p.ylanne@jyu.fi , ritika.sethi@jyu.fi

Keywords: Cell signaling, filamin, microfilaments, NMR, protein-protein interactions, structural biology, x-ray crystallography, x-ray scattering, immunogloblulin-like domain, platelet glycoprotein Ib

Background: Filamins are actin cross-linking and signaling scaffolding proteins that contain mechanically regulated interaction sites in their C-terminus.
Results: Crystal structures of filamin N-terminal domains 3-5 reveal novel domain packing and interaction details of domain 4.
Conclusion: Domain 4 is stabilized by interaction with domain 5.
Significance: Inter-domain interactions positively regulate domain 4 interactions with ligands.

ABSTRACT

Immunoglobulin-like (Ig) domains are a widely expanded superfamily that acts as interaction motifs or as structural spacers in multi-domain proteins. Vertebrate filamins (FLNs), which are multifunctional actin binding proteins, consists of 24 Ig domains. We have recently discovered that in the C-terminal Rod 2 region of FLN, Ig domains interact with each other forming functional domain pairs, where the interaction with signaling and transmembrane proteins is mechanically regulated by weak actomyosin contraction forces. Here, we investigated if there are similar inter-domain interactions around domain 4 in the N-terminal Rod 1 region of FLN. Protein crystal structures revealed a new type of domain organization between domains 3, 4 and 5. In this module, domains 4 and 5 interact rather tightly whereas domain 3 has a partially flexible interface with domain 4. NMR peptide titration experiments showed that within the three domain module, domain 4 is capable for interaction with a peptide derived from platelet glycoprotein Ib. Crystal structure of FLN domains 4 and 5 in complex with the peptide revealed a typical β sheet augmentation interaction observed for many FLN ligands. Domain 5 was found to stabilize domain 4, and this could provide a mechanism for the regulation of domain 4 interactions.

Filamins (FLN) are actin cross-linking proteins that are required for multicellular tissue differentiation. All three FLN genes (FLNA, FLNB and FLNC) are essential in mouse and truncation or substitution mutations cause developmental defects in humans (1, 2) (Figure 1). The diversity of phenotypes caused by FLN mutations can be explained by at least 90 proteins that interact with FLNs (3). The interaction partners can be classified to at least three different categories: transmembrane proteins, cytoskeletal proteins and intracellular signaling proteins. Thus, FLNs are involved in stabilization and regulation of plasma membrane, regulation of actin cytoskeleton and intracellular signaling (3–8).

Structurally, vertebrate FLNs consist of an N-terminal actin-binding domain and 24

immunoglobulin-like (Ig) domains (Figure 1). Domains 1 -15 are referred to as Rod 1 and 16-24 as Rod 2. The structure of actin-binding domain is similar to that of α-actinin and is composed of two calponin homology (CH) domains (9, 10). The FLN Ig domains have a characteristic structure and they can be regarded as protein interaction modules. They often interact with other proteins by a β sheet augmentation mechanism. In this mechanism, the interaction partner forms an additional β -strand next to the strand C of the FLN domain and simultaneously interacts with the hydrophobic groove between the strands C and D, called the CD face (11–14). It is using this mode that ligands like transmembrane receptors of the integrin family (12, 15, 16), the platelet von Willebrand factor receptor subunit glycoprotein Ib (GPIb) (11) and the cystic fibrosis transmembrane conductance regulator (17, 18) interact with FLNa domains 17, 19, 21, and 23. Also, signaling protein FilGAP uses the same mechanism for interacting with FLNa domain 23 (4) and migfilin with FLNa domain 21 (13, 14). Biochemical studies have suggested that also FLNa domain 4 interacts in a similar way with many of the ligands (19). Interestingly, in the dimerization interface of FLNc and FLNa, domain 24 also utilizes the CD face, but the β sheet augmentation occurs through strand D (20, 21).

There are three structurally characterized, closely interacting domain pairs in the C- terminal Rod 2 region of FLNa: domains 16-17, 18-19 and 20-21 (15, 22). Interestingly, in FLNa domain pairs 18-19 and 20-21, the function of the even numbered domain is to mask the CD face of the odd domain (15, 22) and this masking can be relieved by low pico-newton range mechanical forces (23–25). To find out if similar structural mechanisms could regulate the interactions of FLN domain 4, we solved the crystal structures of FLNa domains 3-5, FLNc domains 4-5 and FLNc domains 4-5 in complex with GPIb peptide. These structures disclosed a completely new type of interaction between three Ig domains.

RESULTS

Crystal structures of FLNa domains 3-5 and FLNc domains 4-5 show a novel domain-domain organization

The crystal structures of FLNa domains 3-5 (Figure 2A and Table 2) and FLNc domains 4-5 (Figure 2B and Table 2) disclosed a completely new type of interaction between three Ig domains (Figure 2A) where the interfaces are highly conserved (Figure 3 and Figure S1). The domains interact side-by-side with each other along their β sheets. This leads to a sandwich structure where the β sheets of each domain stack roughly parallel on top of each other (Figure 2A, left side), with domain 3 slightly shifted (Figure 2A, right side). In this arrangement, the interaction between domains 3 and 4 is mediated via the edges of the β sheets whereas domains 4 and 5 interact along three β -strands from each side. The buried interface area is about 500 $Å^2$ and 830 $Å^2$ for domains 3-4 and 4-5 respectively, suggesting that the interaction between 4 and 5 is tighter than the other. There is a large hydrophobic interaction surface between domains 4 and 5 around a Trp residue in the A strand of domain 4 (Trp582 in FLNa and Trp577 in FLNc) (Figure 2C), whereas the interaction between domains 3 and 4 has mostly polar characteristics. The main chain structure of FLNc domains 4-5 is largely identical to FLNa domains (root mean square deviation (rmsd) of 0.66 Å between 165 C-α atoms) (Figure 2B).

The domain-domain interactions observed in these crystal structures are, to our knowledge, unique among the entire Ig superfamily. Therefore, we used several complementary techniques to confirm that the domain arrangement and interactions exist also in solution and are not induced by crystal packing. First, we compared the crystal structures with the SAXS scattering data obtained in solution. The chi values for comparison of calculated scattering from the structures and observed solution scattering profile were 1.13 and 1.80 for FLNa domains 3-5 and FLNc domains 4-5, respectively. The structures fitted well in the SAXS-generated *ab-initio* envelopes (Figure 2D and E). Mutations of the contact residues seen in the crystal structure made the two-domain fragment FLNc4-5 more extended in SAXS and the same mutations also diminished the interaction between individual FLNc domains 4 and 5 in pull-down assays (Table S1 and Figure S2). Comparison of NMR chemical shifts between FLNc domain 5 and the domains 4-5 pair also verified the interaction surface (Figure 4).

In line with the relatively small interaction area between FLNa domains 3 and 4, closer analysis of SAXS data using ensemble optimization methods (EOM) suggested that in both, FLNa and FLNc, three domain fragments of domains 3-5 can be

flexible in solution. This is shown by the broader D_{max} range for three domain fragments as compared to FLNc4-5 (Figure 5 A, B). To further test the flexibility of FLNa3-5 structure, we performed molecular dynamics (MD) simulations on FLNa3-5 without any restraints. Analysis of the snapshot structures obtained from 50 ns MD simulations showed that domain 3 changes its orientations with respect to domain 4 and 5 whose interactions stay intact (Figure 5 C). This flexibility of the three domain fragment observed in the MD simulations is in accordance with the observed solution scattering profile of FLNa3-5 (Chi values for snapshots of two extreme orientations in the range of 1.15 -1.23) and the snapshots fit well in the SAXS-generated *ab-initio* envelopes (Figure 5 D).

Taken together, the crystal structures of FLNa domain 3-5 and FLNc domains 4-5 reveal a new type of Ig-domain packing that fits well with analyses performed in solution stage. The domains 4 and 5 interact relatively tightly whereas the interface between domains 3 and 4 may be partly flexible.

Ligand peptide binds to domain 4 in the three domain module

Earlier, FLNa domain 4, but not 3 and 5, has been shown to interact with β -strand forming peptides (19). In FLNa3-5 and FLNc4-5 structures, the CD surfaces of all three domains are exposed. However, in domains 3 and 5, the CD loop partially occludes the groove between the β -strands (Figure 6A, C), which is not seen in domain 4. This suggests that only domain 4 may interact via its CD face. However, in FLNc domain 4 but not FLNa, the β -strand C is preceded by a 3_{10} helix (Figure 6B) that might interfere with β -strand augmentation interactions. To test if FLNc domain 4 can still bind a ligand, we co-crystallized the FLNc4-5 fragment with the model peptide derived from GPIb, that commonly has the highest interaction affinity among test peptides (19). The structure (Figure 6D and Table 2) revealed that the peptide interacts with the typical β-sheet augmentation mechanism originally discovered for FLNa domain 17 (11) (Figure 6E, F). Interestingly, the electron density for the 3_{10} helix and for the BC loop is not visible in this structure, suggesting local flexibility. We confirmed these interactions in solution by recording ^{15}N- and ^{13}C-HSQC spectra of FLNa3-5 and ^{15}N-HSQC spectra of FLNc4-5 in the presence and absence of the GPIb peptide. Chemical shift perturbations mapped at or close to the CD face of domain 4, indicating that it is available for interaction (Figure 6G, H). This indicates that the novel domain-domain interactions between domains 3-5 do not prevent the binding of small β -strand forming peptides to the CD face of domain 4.

Domains 5 stabilizes the structure of domain 4

Isolated domain 4 has been shown to be partially unstable in previous studies (19). To investigate if neighboring domains have an influence on domain 4 stability, we probed the thermal stability of the domains using a hydrophobic fluoroprobe (Figure 7) (26). Comparison of the temperature dependent dye binding curves shows that isolated domain 4 starts binding the dye in the range of 35-45 ^{o}C whereas domain 5 binds only in the 70-80 ^{o}C range. This indicates that the structure of domain 4 is less stable than domain 5. Furthermore, the dye binding curve of FLNc4-5 shows two transition temperatures. The lower temperature at around 55 ^{o}C is considerable higher than that observed with domain 4 alone, whereas the higher transition temperature is close to that of isolated domain 5. This suggests that domain 5 stabilizes domain 4 in the two domain fragment. A similar curve is seen for FLNc3-5 indicating that domain 3 does not have an additional effect on the stability of domain 4.

DISCUSSION

Traditionally, long multi-domain proteins are thought to work as beads on a string that allow great flexibility, but where individual domains perform their functions largely independent of each other. This seems not to be the case in FLNs. Although FLNs are flexible molecules composed of 24 similar Ig domains, we have earlier reported three functional domain-domain interactions in the C terminal Rod 2 region of FLNa. In this paper, we tested if there are similar inter-domain interactions in the Rod 1 region around domain 4. Our major findings are: 1) Domains 3 and 5 interact with domain 4 and this module of FLN domains 3-5 shows a new type of domain-domain arrangement; 2) We show the details of ligand binding to the CD face of FLN domain 4; and 3) provide evidence of domain 4 stabilization by interactions with neighboring domains. We believe that each of these findings has wide implications to our understanding of the FLN

function. The findings and their implications are discussed below.

Based on the sequence similarity with the pair-forming domains in Rod 2 (19, 27), we hypothesized that domain 4 might be involved in domain-domain interactions. To study this, we crystallized FLNa domains 3-5, and FLNc domains 4-5. The structures revealed a novel type of domain packing that has not been observed in Ig domains before. Typically, FLN-type Ig domains interact with each other via the edges of the β sheets and via loop regions (10, 15, 22). On the other hand, many other Ig domains form dimers by interacting perpendicularly face-to-face along their β sheets (28–30). In the current structures, the domains stack on each other and interact face-to-back so that their β sheets are approximately parallel. Since β sheets are rather flat in the FLN-type Ig domains, this kind of arrangement allows maximal interface surface area. This seems to be true particularly between domains 4 and 5, where the interface is governed by several hydrophobic interactions. These features suggest that the interaction between domains 4 and 5 is rather stable. The interface between domains 3 and 4 is slightly shifted, has smaller area than between 4-5, and is mainly polar. These observations suggest that the 3-4 interface may be more flexible than that of 4-5. This was also supported by analysis of SAXS results using EOM and by MD simulations. Residues on both interfaces are conserved throughout the animal kingdom and thus it is likely that the arrangement of domains 3-5 observed here is a general feature in FLNs.

To study how domain 4 interacts with the GPIb peptide derived from GPIb, which has been previously shown to interact with FLNa domain 4 and other similar domains (19), we co-crystallized the peptide with FLNc domains 4-5 and used NMR methods to verify the interaction site in solution. The crystal structure showed that the interaction of the peptide with FLNc4 is almost identical as with FLNa17 (11): the peptide forms an extra β -strand next to the strand C of domain 4 and interacts hydrophobically with the groove between strands C and D. Using NMR chemical shift perturbation mapping, we were able to show that also in solution the peptide interacts with FLNc4-5 and FLNa3-5 via the CD face of domain 4. This fits well with the observation that in both domains 3 and 5 (FLNa3, FLNa5 and FLNc5), the CD face seems not to be accessible for similar β sheet augmentation interaction because of the CD loop conformation. It is noteworthy that in the unligated FLNc domain 4 there is a 3_{10} helical turn just before strand C that partially occludes the CD groove, but the peptide can induce a conformation change and displace this turn. In the absence of the peptide, NMR spectra revealed two sets of cross peaks that could be assigned to the residues belonging to the 3_{10} helix, suggesting that this structure has conformational flexibility in relatively slow ($k_{ex} < 10^3$ s^{-1}) timescale (Tossavainen et al., unpublished). This 3_{10} helix is not seen in the structure of FLNa domain 4 and the corresponding residues show only a single set of peaks in ^{15}N-HSQC spectrum. Taken together, these results demonstrate that the CD face of domain 4 is the preferred binding site for β -strand forming peptides within the module of FLN domains 3-5 and that this site is accessible for interactions in this module. It is of interest that the spleen tyrosine kinase, Syk, has been reported to interact with FLNa domain 5 (31). In our current structures the CD faces of FLNa and FLNc domain 5 is occluded by the closed conformation of the CD loop. Thus, the current structures suggest that this interaction of Syk with FLNa domain 5 may use other kind of structural mechanism than β sheet augmentation next to strand C.

In the Rod 2 region of FLN the function of domain-domain interactions seems to be to mask the binding sites on domains 19 and 21. This masking can be relieved by mechanical force and thus these domain-domain interactions provide the basis for the mechanosensor function of FLN (5, 23, 25, 32). In the module of domain 3-5, reported here, we do not see this kind of masking of the known interaction site in domain 4. Thus, CD face masking cannot explain the function of this conserved module. An alternative possibility might be similar to the interaction of FILGAP with domain 23 where mechanical forces on FLN may destabilize interactions (24). It has been observed before that FLNa domain 4 is partially unstructured when studied by NMR (19). Here we show by hydrophobic fluoroprobe binding assay that domain 5 is required for stabilization of domain 4. Structurally, this can be explained by the hydrophobic surface in domain 4 (particularly the conserved Trp residue at the domain-domain interface), which may cause problems in domain

folding when not allowed to interact with domain 5.

In conclusion, our results highlight that multiple mechanisms have evolved for the inter-domain interactions in FLNs. We report here the presence of a novel three-domain module between domains 3-5 that is conserved in FLNs and partially flexible. We suggest that one function of the three-domain module is to stabilize domain 4 and to allow its interactions via the previously characterized β -strand augmentation mechanism.

EXERIMENTAL PROCEDURES

Protein Expression and Purification
Fragments of the human FLNc and FLNa cDNA (GenBank AJ012737 and AB593010.1) were PCR amplified according to the predicted domain boundaries (7) and cloned to the GST-fusion protein vector pGTVL1 (Structural Genomics Consortium, University of Oxford) according to the ligation-independent cloning method (33). The final products were verified by DNA sequencing. The proteins were expressed in *Escherichia coli* BL21 Gold cells (Agilent Technologies) at 37 ^{o}C for 4 h with 0.4 mM Isopropyl β-D-1-thiogalactopyranoside (IPTG). The bacterial pellets were lysed using French press. The proteins were captured with Glutathione agarose column (Protino Glutathione Agarose 4B, Macherey-Nagel), released with Tobacco Etch virus protease (Invitrogen, Life technologies) and further purified by size exclusion chromatography with HiLoad 26/60 Superdex 75 column (GE Healthcare) in 100 mM NaCl, 1 mM dithiothreitol (DTT), 20 mM Tris pH 7.5 (FLNc fragments) and 100 mM NaCl, 1 mM DTT, 20 mM Tris pH 8.0 (FLNa fragments). Finally, the proteins were concentrated using Centriprep YM-10000 (Millipore). Mutants were generated using the QuikChange Multi site-directed mutagenesis kit (Agilent Technologies). $^{13}C/^{15}N$–labeled FLNc4-5, FLNc5, and FLNa3-5 were expressed in *E.coli* in standard D-glucose/M9 minimal medium. These proteins were purified in 50 mM sodium phosphate, 100 mM NaCl, 1 mM DTT using the same protocol as described above for the unlabeled fragments.

Protein Crystallography
Crystallization trials with hanging drop vapour diffusion method were set up for the purified recombinant proteins at room temperature. First crystals for FLNc4-5 were obtained in 1.4 M Sodium Potassium Phosphate. The condition was optimized using a gradient of salt concentration and the final crystals were mounted from 1.6 M Sodium Potassium Phosphate. These were first cryo-protected by adding 30% glycerol (final concentration) to the mother liquor and then frozen in liquid nitrogen. The crystals for FLNa3-5 were obtained in 0.1 M Sodium Malonate pH 4, 12% w/v Polyethylene glycol (PEG) 3,350 and were frozen in liquid nitrogen using 0.1 M Sodium Malonate pH 4, 35% w/v Polyethylene glycol 3,350. Equimolar mixture (1 mM each) of FLNc4-5 with GPIb peptide (residues 573-596, numbering according to Uniprot ID P07359) was used to obtain co-crystals in 0.1 M HEPES pH 7.5, 20% w/v PEG 8,000 using 1:2 ratio of protein to mother liquor. The crystals were cryo-protected with 6.6% ethylene glycol and 16.6% glycerol.

The diffraction data were collected at 100 K at the ESRF beamline ID23-1(wavelength = 1.07227 Å) (FLNc4-5) and ID29 (wavelength = 0.976250 Å) (FLNa3-5, FLNc4-5/GPIb). The data were processed with XDS (34) and the structures were solved using molecular replacement with the program Phaser (35) using FLNc23 (PDB ID: 2NQC) chain A as the search model for FLNc4-5, FLNc4-5 (PDB code 3V8O) and FLNc23 (2D7Q) as models for FLNa3-5 structure and FLNc4-5 (PDB code 3V8O) for FLNc4-5/GPIb structure. Refinement and model building were performed by programs Refmac5 (36, 37) and Coot (38) for FLNc4-5 and FLNc4-5/GPIb. The model for FLNa3-5 was built using ARP/wARP 7.3 (39) and Coot and refined using Refmac5. The structure of FLNc4-5 was refined using medium non crystallographic symmetry restraints between chains A and B. Structure factors and coordinates were deposited in the PDB with ID 3V8O (FLNc4-5), 4M9P (FLNa3-5) and 4MGX (FLNc4-5/GPIb). For FLNc4-5, 89.2% of amino acids were in the most favored region, 9.8% in additionally allowed regions and 1 % in generously allowed region of the Ramachandran plot. The values for FLNa3-5 were 92.1, 7.5 and 0.4%, respectively and for FLNc4-5/GPIb, 77.6, 19.0 and 3.4%, respectively. Crystal structure figures were generated using PyMOL. The domain-domain interface was analysed using the PISA server (40). Rendering was done in Chimera (41) according to the sequence alignment made with Clustal Omega (42) using FLNa/b/c3-5,

FLNa3-5 of *M. musculus, G. gallus, D. rerio,* and *D. melanogaster*.

Small-Angle X-Ray Scattering Measurements
Small-angle X-ray scattering (SAXS) data were collected on the EMBL (European Molecular Biology Laboratory) X33 beamline at the DESY, Hamburg (43) (MAR345 image plate, sample-detector distance of 2.7 m and wavelength λ = 0.15 nm, covering the momentum transfer range $0.08 < s < 4.9$ nm^{-1} (where $s = 4\pi \sin(\theta)/\lambda$, 2θ = scattering angle)); MAX IV Laboratory, beamline Cassiopeia I911-SAXS at the MAX II storage ring (Lund, Sweden) (44) (PILATUS 1M image plate, sample-detector distance of 2.2 m and wavelength 0.091 nm, covering the momentum transfer range $0.1 < s < 3$ nm^{-1}) and ESRF (European Synchrotron Radiation Facility), beamline BM29 (45) (PILATUS 1M image plate, sample-detector distance of 2.9 m and wavelength 0.10 nm, covering the momentum transfer range $0.01 < s < 5$ nm^{-1}).The protein concentrations were in the range of 1 - 10 mg/ml in purification buffer supplemented with 10 mM DTT. Buffer subtractions were conducted with either BioXTAS RAW software (46) or ATSAS package program PRIMUS (47) and the scattering intensity (I) was extrapolated to zero solute concentration. The forward scattering I(0) and the radius of gyration (R_g) were calculated using the program GUINIER (48), where at very small angles ($s \times R_g < 1.3$), the scattering intensity:

$$I(s) = I(0)\exp(-1/3(R_g s)^2) \quad (1)$$

The distance distribution functions p(r) and the maximum particle dimensions D_{max} were calculated for all the fragments using program GNOM (49). The molecular mass of the constructs were evaluated by comparing the forward scattering with that from reference solution of bovine serum albumin (BSA) with molecular mass, 66 kDa using the equation:

$$Mw_{sample} = I(0)_{sample} \times Mw_{ref} / I(0)_{ref} . \quad (2)$$

Assuming the samples are monodisperse, Porod's law was applied to find out the excluded volume of the hydrated particle as:

$$V = 2\pi^2 I(0) / \int_0^\infty s^2 I_{exp}(s) ds \quad (3)$$

and to check the S^{-4} decay in scattering intensity at higher angles (50). Kratky plot (51) ($I(s) \times s^2$ versus s) was evaluated to check for the flexibility of the protein at higher scattering angles. The scattering patterns were further used to generate low resolution *ab-initio* models of FLNc4-5 and FLNa3-5 by the program DAMMIF (52) or GASBOR (53). Ten rounds of DAMMIF or GASBOR were done to generate models that were averaged using the program DAMAVER (54) to find the best model with common structural features. The scattering intensities of the crystal structures of FLNc4-5 (Protein Data Bank (PDB) ID: 3V8O) and FLNa3-5 (PDB ID: 4M9P) were calculated using CRYSOL (55) and the superposition of the DAMAVER generated envelope with the respective crystal structures are done with SUPCOMB program of the ATSAS package and the figures are made using PyMOL (Schrödinger LLC, Portland, OR) . To assess the flexibility of domain 3 in the FLNa and FLNc3-5 fragments, the ensemble optimization method (EOM) (56) was used. Similar analysis was performed for FLNc4-5 as an internal control. First, 10,000 randomized models (pool) were generated for each fragment using the native chain option in the program RanCH of the EOM package. The scattering profiles of each of these models were compared to the experimental scattering of respective fragments (FLNa3-5, FLNc3-5 and FLNc4-5). A genetic algorithm was used to select a set of representative models (FLNa3-5 = 24; FLNc3-5 = 18 and FLNc4-5 = 12) from the pool such that the average scattering from the selected models fits the experimental scattering. The results were represented as R_g and D_{max} distribution profiles using GraphPad Prism version 4 for Windows (GraphPad Software Inc., La Jolla, CA).

Protein Interaction Assay
Pull-down assays were performed using GST tagged FLNc4 bound to Glutathione agarose resin. 1 - 20 µM of FLNc5 and FLNc5R755D was allowed to interact for 1 hour at 23 °C after which the resin was washed three times with 500 µl of PBS, 1mM DTT and eluted with 10 µl of the SDS-PAGE sample buffer. Proteins were fractionated by SDS-PAGE and visualized with coomassie-stain. Intensities of the protein bands were quantified by ImageJ (57). Data were plotted using GraphPad Prism version 5 for Windows (GraphPad Software Inc. La Jolla, CA) to produce a non-linear regression curve for one site total and non-specific binding (Specific=Bmax × X/(X+Kd); Nonspecific=NS ×

X + Background, where X = ligand concentration).

ThermoFluor Assay
Thermal stability of FLNc4, FLNc5 and FLNc4-5 was determined using Bio-Rad C1000 thermal cycler, CFx96 Real-Time system. Unfolding of the proteins was monitored using the fluorescent dye SYPRO Orange (Invitrogen) which binds to the hydrophobic core of the protein as it unfolds. A temperature gradient was set up from 20 °C to 95 °C with 0.5 °C/30 seconds increments. Each sample contained 100 μM protein, except FLNc4 (150 μM), and 5X dye in 25 μl total volume.

NMR Experiments
NMR samples were prepared in 50 mM NaH_2PO_4, 100 mM NaCl, 1 mM DTT buffer at pH 7.0. D_2O was added to obtain ~8% solutions. Protein concentrations were 0.4-1.2 mM. Measurement temperature was 28 °C for FLNc5 and FLNc4-5, and 35 °C for FLNa3-5. For the chemical shift assignment HNCACB and CBCA(CO)NH spectra were recorded with a Varian INOVA 500 MHz spectrometer equipped with a ^{15}N, ^{13}C, ^{1}H triple-resonance z-PFG probehead for FLNc5 and with a Varian INOVA 800 MHz spectrometer equipped with a cryogenically cooled, ^{15}N, ^{13}C, ^{1}H triple-resonance z-PFG probehead for FLNc4-5 and FLNa3-5. Peptide binding assays were performed by stepwise addition of the model peptide resulting in approximate concentration ratios of 1 (protein):0 (peptide), 1:0.5, 1:1, 1:2, 1:3 and 1:5. At each step a ^{1}H, ^{15}N HSQC spectrum for the detection of backbone amide group chemical shift changes, and a ^{1}H, ^{13}C HSQC spectrum for the detection of methyl group chemical shift changes in the case of FLNa3-5 was recorded. Chemical shift changes were calculated as $\Delta\delta = ((\Delta\delta_H)^2 + (0.15\times\Delta\delta_N)^2)^{1/2}$. All spectra were processed with Vnmr 6.1C (Varian Inc.) and analysed with Sparky 3.110 (T. D. Goddard and D. G. Kneller, University of California, San Francisco).

Molecular Dynamics Calculations
The x-ray structure of FLNa3-5 (PDB ID: 4M9P) was used as the starting structure for MD simulations. Before energy minimizations and MD simulations, TIP3P water molecules extending 13 Å in all dimensions around the solute and counter ions to obtain neutrality were added with LEAP (58). All energy minimizations and MD simulations were performed with NAMD 2.9 (59) using ff03 force field parameters (60). Before MD simulations, the system was relaxed and equilibrated. First the water molecules and counter-ions were minimized using the steepest descent algorithm (3000 steps) keeping the rest of the system fixed. This was followed by similar minimization but only Cα-atoms were restrained to their crystallographic positions with a harmonic force of 5 kcal mol^{-2} $Å^{-1}$ while the rest of the system moved freely. Before starting the production MD simulations, the equilibrium MD simulations for the whole system with Cα-atoms restrained were performed first at constant volume (for 300 ps) and then at constant pressure (for further 300 ps). Finally the whole system was equilibrated by simulating it at constant pressure without any restrains for 450 ps. After the system was fully equilibrated, the 50 ns production simulation was performed without constraints. Five parallel simulations were performed. During the simulations, the system was kept at constant temperature (300 K) using Langevin damping coefficient of 5 ps^{-1} and constant pressure (1 atm) using a Nose´-Hoover Langevin piston (61) with an oscillation timescale of 200 fs and damping timescale of 100 fs. 2 fs integration time step was used under a multiple time stepping scheme (62), where bonded and short-range interactions were computed every time step and long-range electrostatic interactions every third time step. A cutoff of 12 Å for van der Waals and short-range electrostatic interactions was used. To ensure a smooth cutoff for van der Waals interactions, a switching function was started at 10 Å. Long-range electrostatic interactions were calculated using the particle-mesh Ewald method (63). Periodic boundary conditions were used in all simulations. The SHAKE algorithm was applied to constrain the bonds containing hydrogen atoms (64). Snapshots from trajectories obtained from MD simulation were extracted with PTRAJ in ANTECHAMBER (58).

ACCESSION NUMBERS

The Protein Data Bank (PDB) accession number for the crystal coordinates and structure factors reported in this study are 3V8O (FLNc4-5), 4M9P (FLNa3-5), 4MGX (FLNc4-5/GPIb). Chemical shifts for NMR assignments have been deposited to the BioMagResBank database under accession numbers 19496 (FLNa3-5) and 19495 (FLNc4-5).

SUPPLEMENTAL INFORMATION

Supplemental information includes two figures and one table.

ACKNOWLEDGMENTS

We thank Ms Arja Mansikkaviita for excellent technical assistance. Ms Ulla-Maria Jokipii and Ms Susanna Sinisaari-Kaislo helped in the expression and purification of the proteins. We acknowledge European Molecular Biology Lab (EMBL), European Synchrotron Radiation Facility (ESRF) and MAX-LAB for providing synchrotron access for SAXS and crystal data collection. We express gratitude to Michal J. Gajda (EMBL Hamburg), Matthew Bowler, Adam Round, Petra Pernot (ESRF, Grenoble), Sylvio Haas and Tomás Plivelic (MAX-LAB, Lund) for their assistance during data collection at the beamlines. This work has been funded by Marie Curie Actions FP 7 grant to Initial Training Network MUZIC (Muscle Z-disk Protein Complexes: from atomic structure to physiological function) (RS,JY), the National Doctoral Programme in Informational and Structural Biology (MY), and the Sigrid Juselius Foundation and Academy of Finland (JY: 114713 and 138327, PP: 263794 and 259447). CSC – Finnish IT Center for Science is acknowledged for generous computational grant (OTP: jyy2516 and jyy2586). Biocentrum Helsinki and Biocenter Finland are acknowledged for the NMR infrastructure support.

COMPETING INTERESTS STATEMENT

The authors declare that they have no competing financial interests.

AUTHOR CONTRIBUTIONS

RS, JS, SR and UP performed SAXS experiments, RS, JS and JY solved the crystal structures. HT and PP performed NMR experiments and NMR data analysis. UP performed MD simulations. MY and OTP participated in the analysis of the structures. RS and JY wrote the manuscript. All authors participated in the design of the experiments and writing of the text. All authors approved the final version

REFERENCES

1. Fürst, D.O., Goldfarb, L.G., Kley, R. A, Vorgerd, M., Olivé, M., and Van der Ven, P.F.M. (2012). Filamin C-related myopathies: pathology and mechanisms. *Acta Neuropathol.* **125**, 33-46.

2. Kley, R.A, Serdaroglu-Oflazer, P., Leber, Y., Odgerel, Z., Van der Ven, P.F.M., Olivé, M., Ferrer, I., Onipe, A., Mihaylov, M., Bilbao, J.M., et al. (2012). Pathophysiology of protein aggregation and extended phenotyping in filaminopathy. *Brain* **135**, 2642–2660.

3. Nakamura, F., Stossel, T.P., and Hartwig, J.H. (2011). The filamins: organizers of cell structure and function. *Cell Adh. Migr.* **5**, 160–169.

4. Nakamura, F., Heikkinen, O., Pentikäinen, O.T., Osborn, T.M., Kasza, K.E., Weitz, D. A, Kupiainen, O., Permi, P., Kilpeläinen, I., Ylänne, J., et al. (2009). Molecular basis of filamin A-FilGAP interaction and its impairment in congenital disorders associated with filamin A mutations. *PloS One* **4**, e4928.

5. Razinia, Z., Mäkelä, T., Ylänne, J., and Calderwood, D.A (2012). Filamins in Mechanosensing and Signaling. *Annu. Rev. Biophys.* **41**, 227-246.

6. Zhou, A.-X., Hartwig, J.H., and Akyürek, L.M. (2010). Filamins in cell signaling, transcription and organ development. *Trends Cell Biol.* **20**, 113–123.

7. Flier, A. Van Der, and Sonnenberg, A. (2001). Structural and functional aspects of filamins. *Biochim. Biophys. Acta* **1538**, 99-117.

8. Stossel, T.P., Condeelis, J., Cooley, L., Hartwig, J.H., Schleicher, M., and Shapiro, S.S. (2001). Filamins as integrators of cell mechanics and signalling. *Nat. Rev. Mol. Cell Biol*. **2**, 138–145.

9. Gorlin, J.B., Kwiatkowski, D.J., Biology, C., General, M., Hospital, C., and Division, P.O. (1990). Human Endothelial Actin-binding Protein (ABP-280, Nonmuscle Filamin): A Molecular Leaf Spring. *J. Cell Biol.* **111**, 1089–1105.

10. Ruskamo, S., and Ylänne, J. (2009). Structure of the human filamin A actin-binding domain. *Acta Crystallogr. D Biol. Crystallogr.* **65**, 1217–1221.

11. Nakamura, F., Pudas, R., Heikkinen, O., Permi, P., Kilpeläinen, I., Munday, A.D., Hartwig, J.H., Stossel, T.P., and Ylänne, J. (2006). The structure of the GPIb-filamin A complex. *Blood* **107**, 1925–1932.

12. Kiema, T., Lad, Y., Jiang, P., Oxley, C.L., Baldassarre, M., Wegener, K.L., Campbell, I.D., Ylänne, J., and Calderwood, D.A. (2006). The Molecular Basis of Filamin Binding to Integrins and Competition with Talin. Mol. Cell *21*, 337–347.

13. Lad, Y., Jiang, P., Ruskamo, S., Harburger, D.S., Ylanne, J., Campbell, I.D., and Calderwood, D. A. (2008). Structural Basis of the Migfilin-Filamin Interaction and Competition with Integrin Tails. *J. Biol. Chem.* **283**, 35154–35163.

14. Ithychanda, S.S., Das, M., Ma, Y.-Q., Ding, K., Wang, X., Gupta, S., Wu, C., Plow, E.F., and Qin, J. (2009). Migfilin, a molecular switch in regulation of integrin activation. *J. Biol. Chem.* **284**, 4713–4722.

15. Heikkinen, O.K., Ruskamo, S., Konarev, P. V, Svergun, D.I., Iivanainen, T., Heikkinen, S.M., Permi, P., Koskela, H., Kilpeläinen, I., and Ylänne, J. (2009). Atomic structures of two novel immunoglobulin-like domain pairs in the actin cross-linking protein filamin. *J. Biol. Chem.* **284**, 25450–25458.

16. Takala, H., Nurminen, E., Nurmi, S.M., Aatonen, M., Strandin, T., Takatalo, M., Kiema, T., Gahmberg, C.G., Ylänne, J. and Fagerholm, S.C. (2008). Beta2 integrin phosphorylation on Thr758 acts as a molecular switch to regulate 14-3-3 and filamin binding. *Blood* **112**, 1853–1862.

17. Smith, L., Page, R.C., Xu, Z., Kohli, E., Litman, P., Nix, J.C., Ithychanda, S.S., Liu, J., Qin, J., Misra, S., et al. (2010). Biochemical Basis of the Interaction between Cystic Fibrosis Transmembrane Conductance Regulator and Immunoglobulin-like Repeats of Filamin. *J. Biol. Chem.* **285**, 17166–17176.

18. Playford, M.P., Nurminen, E., Pentikäinen, O.T., Milgram, S.L., Hartwig, J.H., Stossel, T.P., and Nakamura, F. (2010). Cystic fibrosis transmembrane conductance regulator interacts with multiple immunoglobulin domains of filamin A. *J. Biol. Chem.* **285**, 17156–17165.

19. Ithychanda, S.S., Hsu, D., Li, H., Yan, L., Liu, D.D., Liu, D., Das, M., Plow, E.F., and Qin, J. (2009b). Identification and characterization of multiple similar ligand-binding repeats in filamin: implication on filamin-mediated receptor clustering and cross-talk. *J. Biol. Chem.* **284**, 35113–35121.

20. Pudas, R., Kiema, T.-R., Butler, P.J.G., Stewart, M., and Ylänne, J. (2005). Structural basis for vertebrate filamin dimerization. *Structure* **13**, 111–119.

21. Seo, M.-D., Seok, S.-H., Im, H., Kwon, A.-R., Lee, S.J., Kim, H.-R., Cho, Y., Park, D., and Lee, B.-J. (2009). Crystal structure of the dimerization domain of human filamin A. *Proteins* **75**, 258–263.

22. Lad, Y., Kiema, T., Jiang, P., Pentikäinen, O.T., Coles, C.H., Campbell, I.D., Calderwood, D. A, and Ylänne, J. (2007). Structure of three tandem filamin domains reveals auto-inhibition of ligand binding. *EMBO J.* **26**, 3993–4004.

23. Pentikäinen, U., and Ylänne, J. (2009). The regulation mechanism for the auto-inhibition of binding of human filamin A to integrin. *J. Mol. Biol.* **393**, 644–657.

24. Ehrlicher, A. J., Nakamura, F., Hartwig, J.H., Weitz, D.A, and Stossel, T.P. (2011). Mechanical strain in actin networks regulates FilGAP and integrin binding to filamin A. *Nature* **478**, 260–263.

25. Rognoni, L., Stigler, J., Pelz, B., Ylanne, J., and Rief, M. (2012). Dynamic force sensing of filamin revealed in single-molecule experiments. *Proc. Natl. Acad. Sci.* **21**, 1–6.

26. Pantoliano, M. W., Petrella, E. C., Kwasnoski, J. D., Lobanov, V. S., Myslik, J., Graf, E., Carver, T., Asel, E., Springer, B. A., Lane, P., and Salemme, F. R. (2001). High-density miniaturized thermal shift assays as a general strategy for drug discovery. *J. Biomol. Screen*. **6**, 429–440.

27. Light, S., Sagit, R., Ithychanda, S.S., Qin, J., and Elofsson, A. (2012). The evolution of filamin - a protein domain repeat perspective. *J. Struct. Biol.* **179**, 289–298.

28. Wurzburg, B. A, and Jardetzky, T.S. (2009). Conformational flexibility in immunoglobulin E-Fc 3-4 revealed in multiple crystal forms. *J. Mol. Biol.* **393**, 176–190.

29. Müller, R., Gräwert, M. A, Kern, T., Madl, T., Peschek, J., Sattler, M., Groll, M., and Buchner, J. (2013). High-resolution structures of the IgM Fc domains reveal principles of its hexamer formation. *Proc Natl Acad Sci U S A*. **110**, 10183–10188.

30. Biersmith, B.H., Hammel, M., Geisbrecht, E.R., and Bouyain, S. (2011). The immunoglobulin-like domains 1 and 2 of the protein tyrosine phosphatase LAR adopt an unusual horseshoe-like conformation. *J. Mol. Biol.* **408**, 616–627.

31. Falet, H., Pollitt, A.Y., Begonja, A.J., Weber, S.E., Duerschmied, D., Wagner, D.D., Watson, S.P., and Hartwig, J.H. (2010). A novel interaction between FlnA and Syk regulates platelet ITAM-mediated receptor signaling and function. *J. Exp. Med.* **207**, 1967–1979.

32. Chen, H., Chandrasekar, S., Sheetz, M.P., Stossel, T.P., Nakamura, F., and Yan, J. (2013). Mechanical perturbation of filamin A immunoglobulin repeats 20-21 reveals potential non-equilibrium mechanochemical partner binding function. *Sci Rep.* **3**, 1642.

33. Gileadi, O., Burgess-brown, N.A., Colebrook, S.M., Berridge, G., Savitsky, P., Smee, C.E.A., Loppnau, P., Johansson, C., Salah, E., and Pantic, N.H. (2007). High Throughput Production of Recombinant Human Proteins for Crystallography. *Methods Mol. Biol.* **426**, 221–246.

34. Kabsch, B.Y.W. (1993). Automatic Processing of Rotation Diffraction Data from Crystals of Initially Unknown Symmetry and Cell Constants. *J. Appl. Cryst.* **26**, 795–800.

35. McCoy, A.J., Grosse-Kunstleve, R.W., Adams, P.D., Winn, M.D., Storoni, L.C., and Read, R.J. (2007). Phaser crystallographic software. *J. Appl. Crystallogr.* **40**, 658–674.

36. Murshudov, G.N., Vagin, A.A., and Dodson, E.J. (1997). Refinement of macromolecular structures by the maximum-likelihood method. *Acta Crystallogr. D Biol. Crystallogr.* **53**, 240–255.

37. Winn, M.D., Charles, C., Cowtan, K.D., Dodson, E.J., Leslie, A.G.W., Mccoy, A., Stuart, J., Garib, N., Powell, H.R., and Randy, J. (2011). Overview of the CCP4 suite and current developments. *Acta Crystallogr. D Biol. Crystallogr.* **4449**, 235–242.

38. Emsley, P., and Cowtan, K. (2004). Coot : model-building tools for molecular graphics. *Acta Crystallogr. D Biol. Crystallogr.* **60**, 2126–2132.

39. Langer, G. G, Cohen, S., Lamzin, V. S., Perrakis, A. (2008). Automated macromolecular model building for X-ray crystallography using ARP/wARP version 7. *Nat Protoc.* **3**, 1171–1179.

40. Krissinel, E., and Henrick, K. (2007). Inference of macromolecular assemblies from crystalline state. *J. Mol. Biol.* **372**, 774–797.

41. Pettersen, E. F., Goddard, T. D., Huang, C. C., Couch, G. S., Greenblatt, D. M., Meng, E. C., and Ferrin, T. E. (2004). UCSF Chimera--a visualization system for exploratory research and analysis. *J Comput. Chem.* **25**, 1605–1612.

42. Sievers, F., Wilm, A., Dineen, D., Gibson, T. J., Karplus, K., Li, W., Lopez, R., McWilliam, H., Remmert, M., Söding, J., Thompson, J. D., and Higgins, D. G. (2011). Fast, scalable generation of high-quality protein multiple sequence alignments using Clustal Omega. *Mol. Syst. Biol.* **7**, 1-6.

43. Roessle, M.W., Klaering, R., Ristau, U., Robrahn, B., Jahn, D., Gehrmann, T., Konarev, P., Round, A., Fiedler, S., Hermes, C., et al. (2007). Upgrade of the small-angle X-ray scattering beamline X33 at the European Molecular Biology Laboratory, Hamburg. *J. Appl. Crystallogr.* **40**, s190–s194.

44. Labrador, A., Cerenius, Y., Svensson, C., Theodor, K., and Plivelic, T. (2013). The yellow mini-hutch for SAXS experiments at MAX IV Laboratory. *J. Phys.: Conf. Ser.* **425**, 072019.

45. Pernot, P., Round, A., Barrett, R., De Maria Antolinos, A., Gobbo, A., Gordon, E., Huet, J., Kieffer, J., Lentini, M., Mattenet, M., et al. (2013). Upgraded ESRF BM29 beamline for SAXS on macromolecules in solution. *J Synchrotron Radiat.* **20**, 660–664.

46. Nielsen, S. S., Toft, K. N., Snakenborg, D., Jeppesen, M. G., Jacobsen, J. K., Vestergaard, B., Kutter., J.P. and Arleth, L. (2009). BioXTAS RAW, a software program for highthroughput automated small-angle X-ray scattering data reduction and preliminary analysis. *J. Appl. Cryst.* **42**, 959–964.

47. Konarev, P. V., Volkov, V. V., Sokolova, A. V., Koch, M.H.J., and Svergun, D.I. (2003). PRIMUS : a Windows PC-based system for small-angle scattering data analysis. *J. Appl. Crystallogr.* **36**, 1277–1282.

48. Guinier, A. (1939). La diffraction des rayons X aux très petits angles: application à l'étude de phénomènes ultramicroscopiques. *Ann. Phys.* **12**, 161–237.

49. Svergun, D.I. (1992). Determination of the regularization parameter in indirect-transform. *J. Appl. Cryst.* **25,** 495–503.

50. Rambo, R.P., and Tainer, J. A (2011). Characterizing flexible and intrinsically unstructured biological macromolecules by SAS using the Porod-Debye law. *Biopolymers* **95**, 559–571.

51. Kratky, O., and Glatter, O. (1982). Small Angle X-ray Scattering (Academic Press, London).

52. Franke, D., and Svergun, D.I. (2009). DAMMIF, a program for rapid ab-initio shape determination in small-angle scattering. *J. Appl. Cryst.* **42**, 342–346.

53. Svergun, D.I., Petoukhov, M. V, and Koch, M.H. (2001). Determination of domain structure of proteins from X-ray solution scattering. *Biophys. J.* **80**, 2946–2953.

54. Volkov, V. V., and Svergun, D.I. (2003). Uniqueness of ab initio shape determination in small-angle scattering. *J. Appl. Cryst.* **36**, 860–864.

55. Svergun, D., Barberato, C. and Koch, M.H.J. (1995). CRYSOL – a Program to Evaluate X-ray Solution Scattering of Biological Macromolecules from Atomic Coordinates. *J. Appl. Cryst.* **28**, 768–773.

56. Bernadó, P., Mylonas, E., Petoukhov, M. V., Blackledge, M., and Svergun, D.I. (2007). Structural Characterization of Flexible Proteins Using Small-Angle X-ray Scattering. *J Am Chem Soc.* **129**, 5656–5664.

57. Schneider, C.A., Rasband, W.S., and Eliceiri, K.W. (2012). NIH Image to ImageJ: 25 years of image analysis. *Nat. Methods* **9**, 671–675.

58. Wang, J., Wang, W., Kollman, P. A. and Case, D. A. (2006) Automatic atom type and bond type perception in molecular mechanical calculations. *J. Mol. Graphics Modell.* **25**, 247–260.

59. Phillips, J.C., Braun, R., Wang, W., Gumbart, J., Tajkhorshid, E., Villa, E., Chipot, C., Skeel, R.D., Kalé, L. and Schulten, K. (2005). Scalable molecular dynamics with NAMD. *J. Comput. Chem.* **26** 1781–1802.

60. Duan, Y., Wu, C., Chowdhury, S., Lee, M. C., Xiong, G., Zhang, W., Yang, R., Cieplak, P., Luo, R., Lee, T., Caldwell, J., Wang, J. and Kollman, P. (2003). A point-charge force field for molecular mechanics simulations of proteins based on condensed-phase quantum mechanical calculations. *J. Comput. Chem.* **24**, 1999–2012.

61. Feller, S.E., Zhang, Y.H., Pastor, R.W. and Brooks, B.R. (1995). Constant pressure molecular dynamics simulation: the Langevin piston method. *J Chem Phys.* **103**, 4613–4621.

62. Schlick, T., Skeel, R., Brunger, A.T.D., Kale, L.V., Board, J.A. Jr., Hermans, J. and Schulte, K. (1999). Computational modeling predicts the structure and computational molecular biophysics. J. *Comput. Phys.* **151**, 9–48.

63. Darden, T., York, D. and Pedersen, L. (1993). Partiicle mesh Ewald-an N Log(N) method for Ewald sums in large systems. *J. Chem. Phys.* **98**, 10089–10092.

64. Ryckaert, J., Ciccotti, G. and Berendsen, H.J. (1977). Numerical integration of the Cartesian equations of motion of a system with constraints: molecular dynamics of n-alkanes. *J. Comput. Phys.* **23**, 327–341.

FIGURE LEGENDS

Figure 1 Schematic representation of filamin dimer structure: Actin Binding Domains (ABDs) are red, followed by 24 Ig domains. Three known domain pairs in the Rod 2 region (16-17, 18-19 and 20-21) are shown in green, purple and orange, respectively. The fragments of the Rod 1 region investigated in this study are labeled on the right subunit. Isoform specific (FLNA, FLNB and FLNC) substitution and local deletion mutations in human patients are shown on the left subunit.

Figure 2 New domain packing in FLNs**:** **(A)** Two views of the crystal structure of FLNa3-5, where domains 3, 4 and 5 are shown in yellow, green and cyan, respectively. β -strands C and D are shown in red; **(B)** Superposition of FLNc4-5 (orange) with FLNa4-5 (domain coloring as in panel A); **(C)** Zoom-in view of the interface showing key residues; **(D, E)** Superposition of the FLNc4-5 and FLNa3-5 structures with their respective *ab-initio* SAXS envelopes. Normalized Spatial Discrepancy (NSD) of superposition for FLNc4-5 is 2.41 and for FLNa3-5 is 1.63.

Figure 3 Surface conservation of the domain-domain interfaces in FLN3-5. Corresponding cartoon models made using PyMOL are shown below the surface visualization. Sequence alignment is shown in Figure S1.

Figure 4 NMR data showing interaction between domains 4 and 5 in solution: (**A)** HSQC peaks of residues marked in orange have different chemical shifts in the spectra of FLNc5 and FLNc4-5; **(B)** Plot of the FLNc5 residues showing chemical shifts as compared to FLNc4-5. Further confirmation of the interface is shown in Figure S2 and Table S1.

Figure 5 EOM and MD data showing the flexibility of the three domain fragment: **(A)** R_g and **(B)** D_{max} of the pools (dashed lines) and the selected models (solid lines) for FLNa3-5 (green), FLNc3-5 (black) and FLNc4-5 (red) as internal control. Note that the selected models of FLNc4-5 have a narrow R_g and D_{max} distribution whereas the selected models of FLNc3-5 and FLNa3-5 show a broader distribution. This suggests that there is more flexibility between domains 3-4 than between domains 4-5; **(C)** The superposition of FLNa3-5 crystal structure (domain 3, in yellow) with two snapshots from MD simulations (one snapshot with domain 3 in orange and the second snapshot with domain 3 in magenta). Domains 4 and 5 are shown in grey for crystal structure and MD snapshots and are superimposed using VERTAA module in Bodil (Lehtonen et al., 2004). The snapshot structures shown represent the most extreme orientations between which domain 3 oscillates during MD simulations; **(D)** Superposition of one snapshot structure (orange) from MD simulations of FLNa3-5 with the SAXS generated *ab-initio* envelope (NSD of superposition is 2.05).

Figure 6 CD face conformation and interactions: **(A, B, C)** Conformation of the CD face (red) of individual domains. **(A)** FLNa3; **(B)** FLNa4 (green) and FLNc4 (grey). 3_{10} helix of FLNc4 is labeled; **(C)** FLNa5 (cyan) and FLNc5 (grey); Closed conformation of the CD loop is marked with an arrow; **(D)** Co-crystal structure of FLNc4-5 with GPIb peptide (orange); **(E)** Superposition of FLNc4 and GPIb peptide with FLNa17 (grey) and GPIb peptide (magenta) (rmsd = 0.75 Å between 89 C-α atoms); **(F)** Detailed view of the peptide conformation with FLNc4 (peptide in orange) and with FLNa17 (peptide in magenta); **(G)** NMR titration of GPIb with FLNa3-5: Residues undergoing

changes in peak intensity and chemical shifts are shown as red (amide group changes) and pink side chains (methyl group changes); **(H)** Residues mapped for the GPIb interaction with FLNc4: peaks vanish (red), chemical shift difference more than 0.025 ppm (orange)

Figure 7 Thermal stability assay showing domain 5 stabilizes domain 4: Temperature dependent fluoroprobe binding curves of FLNc4 (black), FLNc5 (green), FLNc4-5 (magenta) and FLNc3-5(orange) are shown.

Table 1: Parameters derived from SAXS measurements of FLN domains 4-5 and FLN 3-5.

Protein	**$^{\S}R_g$ (nm)**	**$\tilde{}D_{max}$ (nm)$^{\$\$}$**
FLN domains 4-5 constructs		
FLNc4-5	1.71 ± 0.01	4.8
FLNa4-5	1.90 ± 0.01	5.3
FLN domains 3-5 constructs		
FLNa 3-5	2.32$^{\#}$	7.7$^{\#}$
FLNc 3-5	2.41$^{\#}$	7.9$^{\#}$

§**R_g:** Radius of Gyration (mean square of the distances from the centre of mass of the particle weighted by electron densities) from equation (1); **$\tilde{}D_{max}$:** Maximum dimension inside the particle estimated from distance distribution probability function. $^{\$\$}$ The values written here are with an approximate error of 0.5 nm.
$^{\#}$ These are the average values reported using EOM.

Table 2. Crystallography data collection and refinement statistics

	FLNc4-5 (PDB ID: 3V8O)	**FLNa3-5 (PDB ID: 4M9P)**	**FLNc4-5/GPIb (PDB ID: 4MGX)**
Data collection			
Space group	P $2_12_12_1$	$P6_5$	$P4_322$
Cell dimensions			
a, b, c, Å	63.62, 91.35, 103.72	63.04, 63.04, 136.60	111.80, 111.80, 59.88
α, β, γ, degree	90, 90, 90	90, 90, 120	90, 90, 90
Resolution range, Å	46.63 - 2.8 (2.87 - 2.8)[#]	42.65 - 1.72 (1.76 - 1.72)	47.73 - 3.16 (3.24 - 3.16)
Rsym*,%	15.8 (76.3)	9.7 (67.9)	20.5 (242.7)
I/σI	9.92 (2.7)	18.24 (3.3)	9.53 (0.7)
Completeness, %	100 (98)	99.7 (96.5)	98.2 (100)
Redundancy	4.2 (4.2)	10.9 (8.0)	10.42 (7.8)
Refinement			
Resolution, Å	46.63 - 2.8 (2.87 - 2.8)	42.65 - 1.72 (1.76 - 1.72)	47.73 - 3.16 (3.24 - 3.16)
No. of reflections			
Refinement	13602 (1012)	30839 (1623)	6556 (456)
Test set	1512 (113)	2204 (115)	345 (24)
Rwork /Rfree ,%	20/25.5 (33.4/40.1)	19.9/24.3 (24.5/30.6)	22.6/27.7 (35.9/45.6)
No. of atoms			
Protein	2854	2173	1439
Heterogen	1	null	null
Solvent	47	219	2
Root mean square differences			
Bond lengths, Å	0.022	0.019	0.012
Bond angles, degree	1.8	1.98	1.80
Average B-factor, $Å^2$	29.3	22.18	108.48
Protein	29.28	21.95	108.45
Solvent	23.41	27.04	108.45

Values of the last resolution shell in parentheses

* Diederichs and Karplus (1997)

Figure 1

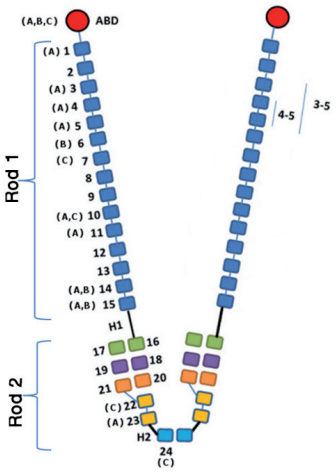
(A,B,C)
ABD
(A) 1
2
(A) 3
(A) 4
(A) 5
(B) 6
(C) 7
8
9
(A,C) 10
(A) 11
12
13
(A,B) 14
(A,B) 15
H1
16
17
18
19
20
21
(C) 22
(A) 23
H2
24
(C)
Rod 1
Rod 2
4-5
3-5

Figure 2

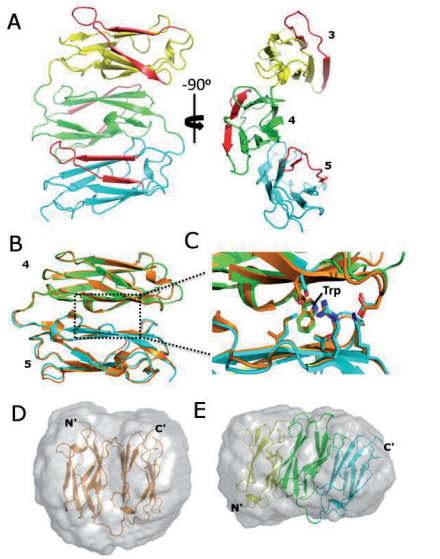

Figure 3

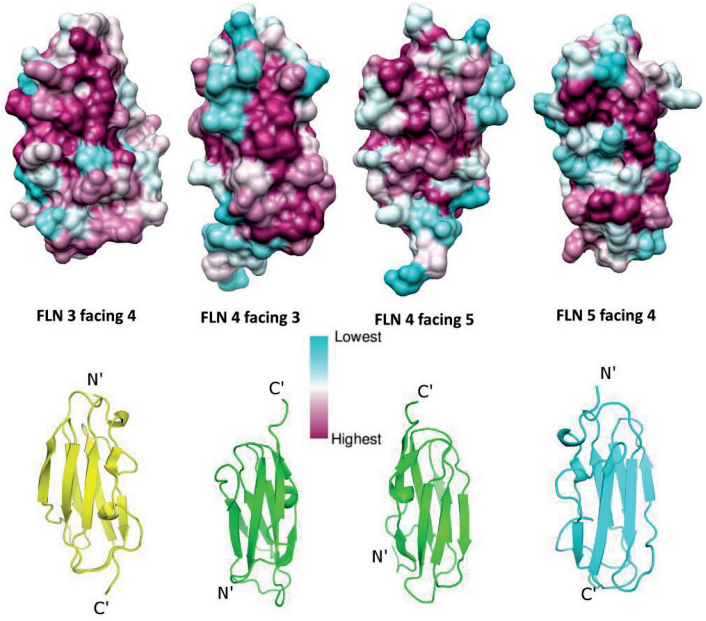
FLN 3 facing 4
FLN 4 facing 3
FLN 4 facing 5
FLN 5 facing 4
Lowest
Highest
N'
C'
C'
N'
C'
N'
N'
C'

Figure 4

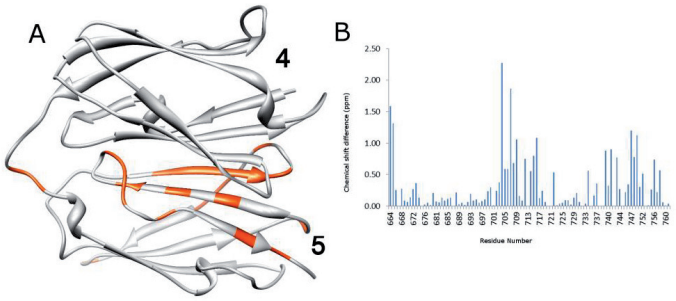
A
4
5
B
Chemical shift difference (ppm)
2.50
2.00
1.50
1.00
0.50
0.00
664
668
672
676
681
685
689
693
697
701
705
709
713
717
721
725
729
733
737
740
744
747
752
756
760
Residue Number

Figure 5

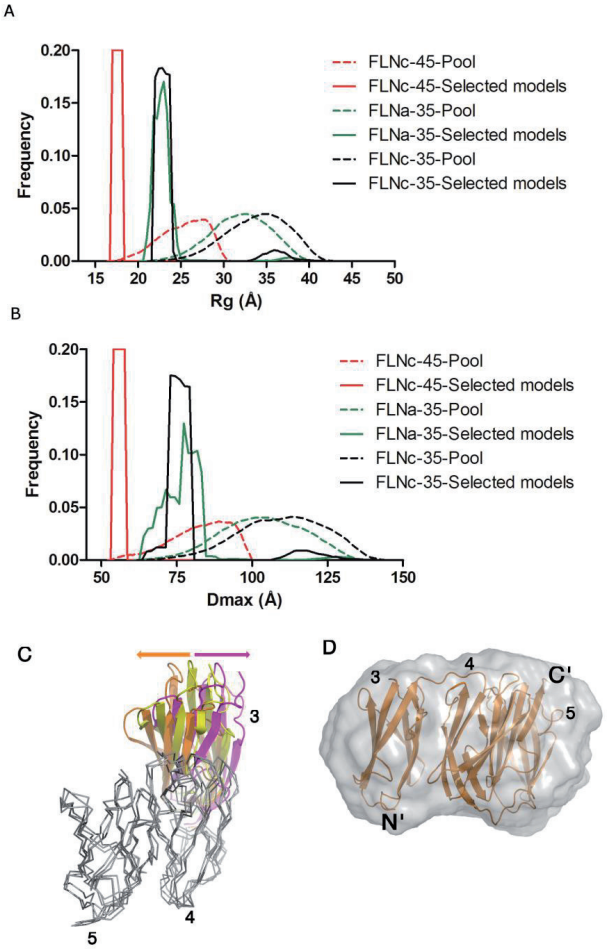
A
Frequency
Rg (Å)
FLNc-45-Pool
FLNc-45-Selected models
FLNa-35-Pool
FLNa-35-Selected models
FLNc-35-Pool
FLNc-35-Selected models
B
Frequency
Dmax (Å)
FLNc-45-Pool
FLNc-45-Selected models
FLNa-35-Pool
FLNa-35-Selected models
FLNc-35-Pool
FLNc-35-Selected models
C
3
4
5
D
3
4
C'
5
N'

Figure 6

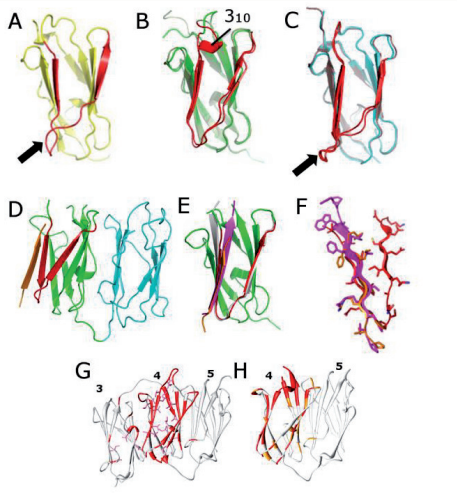

Figure 7

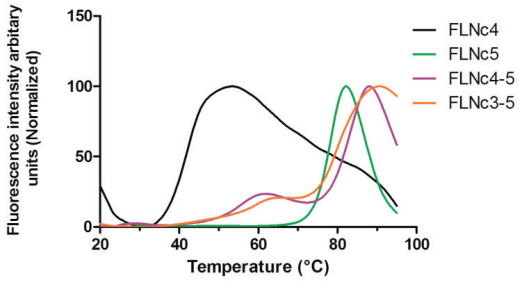
Fluorescence intensity arbitary units (Normalized)
150
100
50
0
20
40
60
80
100
Temperature (°C)
FLNc4
FLNc5
FLNc4-5
FLNc3-5

Supplemental information

A Novel Structural Unit in the N-Terminal Region of Filamins

Ritika Sethi, Jonne Seppälä, Helena Tossavainen, Mikko Ylilauri, Salla Ruskamo, Olli T. Pentikäinen, Ulla Pentikäinen, Perttu Permi, and Jari Ylänne

Inventory of Supplemental information

Figure S1. Residue conservation in FLN 3-5. Related to Figure 3.

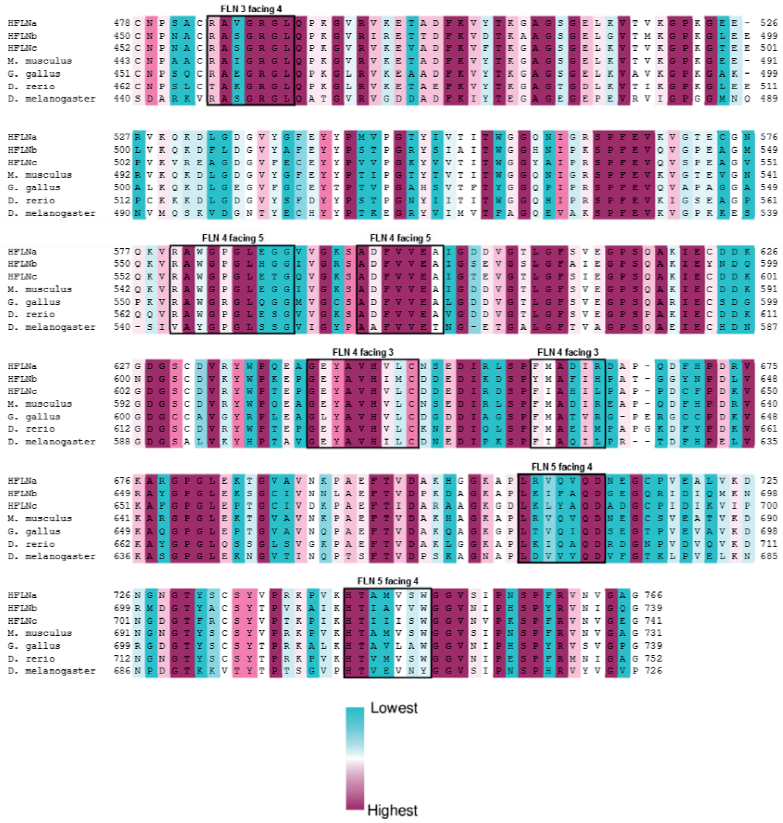

Sequence alignment with the same color code as Figure 3 is shown with the interfaces highlighted with a black box

Figure S2. Overlay of the ^{1}H- ^{15}N HSQC spectra of FLNc5 (red) with FLNc4-5 (blue). Related to Figure 4C.

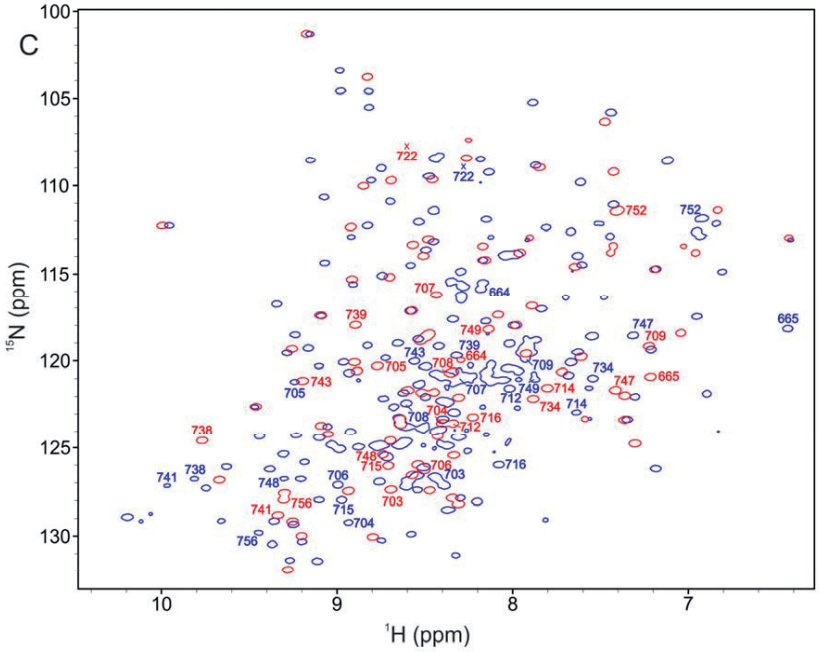

The residues shown in blue in Figure 4C are labeled here. The peaks of residue 722 are visible at a lower contour level and their positions are marked with crosses.

Figure S3. **^{1}H- ^{15}N HSQC spectra overlay: (A) FLNa3-5 + GPIb peptide; and (B) FLNc4-5 + GPIb peptide (Related to Figure 6G and H)**

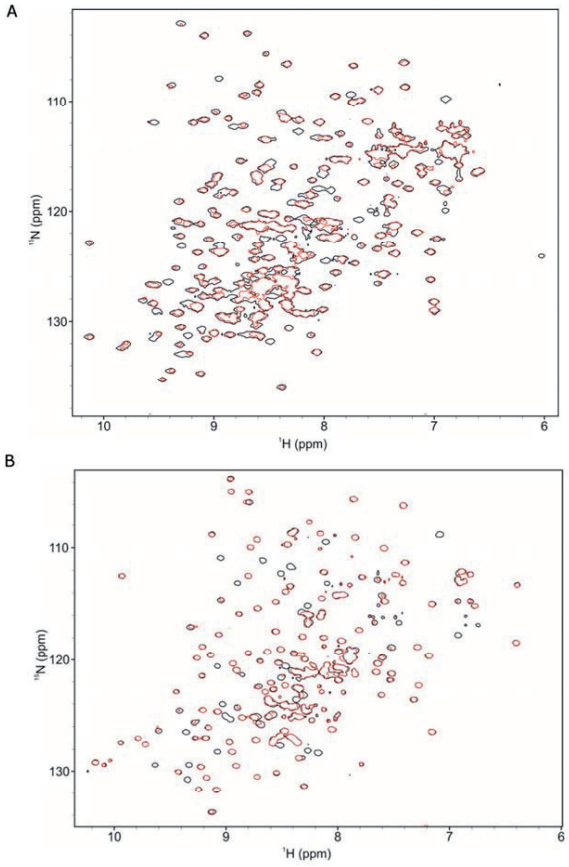

The black peaks represent the ^{15}N HSQC spectrum of the protein alone. Overlaid with this is the 1:1 protein:peptide ^{15}N HSQC spectrum represented with red peaks.

II

FLEXIBLE STRUCTURE OF PEPTIDE-BOUND FILAMIN A MECHANOSENSOR DOMAIN PAIR 20–21

by

Jonne Seppälä, Helena Tossavainen, Nebojsa Rodic, Perttu Permi, Ulla Pentikäinen, and Jari Ylänne

Submitted manuscript

III

STRUCTURAL CHARACTERIZATION OF HUMAN FILAMIN DOMAINS 16–17 PATIENT MUTATIONS CAUSING SKELETAL DYSPLASIA

by

Jonne Seppälä, Tatu Haataja, Jari Ylänne, and Ulla Pentikäinen

Manuscript